

Terahertz aqueous photonics

Qi JIN, Yiwen E, Xi-Cheng ZHANG (✉)

The Institute of Optics, University of Rochester, Rochester, NY 14627, USA

© Higher Education Press 2020

Abstract Developing efficient and robust terahertz (THz) sources is of incessant interest in the THz community for their wide applications. With successive effort in past decades, numerous groups have achieved THz wave generation from solids, gases, and plasmas. However, liquid, especially liquid water has never been demonstrated as a THz source. One main reason leading the impediment is that water has strong absorption characteristics in the THz frequency regime.

A thin water film under intense laser excitation was introduced as the THz source to mitigate the considerable loss of THz waves from the absorption. Laser-induced plasma formation associated with a ponderomotive force-induced dipole model was proposed to explain the generation process. For the one-color excitation scheme, the water film generates a higher THz electric field than the air does under the identical experimental condition. Unlike the case of air, THz wave generation from liquid water prefers a sub-picosecond (200–800 fs) laser pulse rather than a femtosecond pulse (~50 fs). This observation results from the plasma generation process in water.

For the two-color excitation scheme, the THz electric field is enhanced by one-order of magnitude in comparison with the one-color case. Meanwhile, coherent control of the THz field is achieved by adjusting the relative phase between the fundamental pulse and the second-harmonic pulse.

To eliminate the total internal reflection of THz waves at the water-air interface of a water film, a water line produced by a syringe needle was used to emit THz waves. As expected, more THz radiation can be coupled out and detected. THz wave generation from other liquids were also tested.

Keywords terahertz (THz) wave generation, liquid water, laser-induced plasma

1 Introduction

1.1 Properties and applications of terahertz waves

Many molecules have spectral features in the terahertz (THz) frequency band due to absorption and scattering caused by molecular oscillation and rotation. Thus, identifying the composition of a material is an important application for THz spectroscopy. One popular technique developed for this purpose is called THz time-domain spectroscopy (THz-TDS) [1]. Figure 1 shows a typical arrangement of a THz-TDS system. A laser beam is split into two parts by a beam splitter (BS). The pump beam is used to excite the THz emitter to generate THz radiation while the probe beam detects the signal that is proportional to the electric field of the THz pulse. The time delay between the two beams is controlled by a mechanical translation stage. The measurement of THz waveforms happens when the generated THz pulse and the probe pulse both reach the receiver. Since the laser pulse oscillates much faster than the THz pulse does, the receiver can be regarded as an ultrafast gated detector. The probe laser

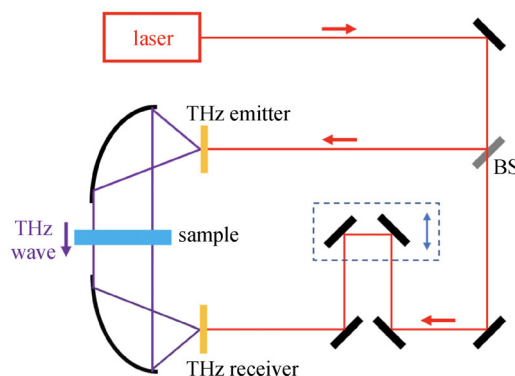


Fig. 1 A generic arrangement for a THz time-domain spectroscopy (THz-TDS) system. Pulses from the femtosecond laser are split at the beam splitter (BS). There is a delay stage used to alter the time of arrival at the THz receiver between the THz pulse and the laser pulse

pulse with the gated nature samples the waveform of the THz electric field. When the unidentified sample is placed in the THz beam path, the THz signal that carries the sample's information will be sensed. To obtain the true contribution from the sample, a reference signal with no sample presented has to be recorded. Compared to the reference signal, the signal from the sample usually has a reduced amplitude, a time shift, and oscillations in its tail. The reduced amplitude results from the absorption for THz waves. The time shift indicates that the THz waves pass through a material with a refractive index greater than the index of refraction of air. The oscillations have the feature of resonant absorption.

The timescale of THz waves is around one picosecond, making it a great tool in pump-probe experiments to study ultrafast phenomena such as electron oscillation and molecular rotation [2].

The wavelength of THz waves ranges from hundreds of microns to a few millimeters. The wavelength of an electromagnetic wave determines its interaction with a physical structure. Absorption and scattering will occur if the wavelength is comparable with the dimension of the structure. Otherwise, there will be no substantial interaction. The long wavelength of THz waves leads to little attenuation when THz waves pass through many dielectric materials, such as paper, wood, plastic, clothing, and glass. Therefore, THz waves can be used for the imaging of opaque objects [3,4]. In addition, THz radiation is the ideal source for imaging in some poor environmental conditions (such as dense smoke and dust).

A THz photon has an energy level of meV. This photon energy is lower than the energy of chemical bonds, assuring that THz radiation induces no destruction from the interaction. As a comparison, the photon energy of X-rays ranges from 100 eV to 100 keV, which can be harmful to bio-medical samples and human beings. The safety of THz radiation is a requisite for its applications in nondestructive evaluation and safety check.

1.2 Pulsed THz sources

1.2.1 Photoconductive antenna

A photoconductive antenna (PCA) is also known as a photoconductive switch or an Auston switch. It is one of the most widely used devices for THz wave generation and detection. A PCA is usually composed of two metal electrodes deposited on a semiconductor substrate (such as low-temperature grown GaAs [5,6]). If a femtosecond optical pulse with photon energy greater than the bandgap of the semiconductor is focused onto the gap between the two electrodes, electron-hole pairs will be produced. The density of these charged particles will rapidly increase to “turn on” the switch. Free carriers are then accelerated by the electric field generated from an applied DC voltage

between the two electrodes. Occurred transient photocurrents in this process result in the radiation of electromagnetic waves. When the PCA is switched by a femtosecond pulse, the transient current has a picosecond timescale leading to the emission of a THz pulse.

THz wave generation from a PCA is the most popular approach used in commercial THz products because it does not require intense optical pulses for excitation. As a compromise, a high external voltage is a requisite to build the electric field between the electrodes for the generation of THz pulses. Besides the possibility of causing a breakdown in the substrate, a high bias voltage will lead to a large amount of electric noise that harms the system.

1.2.2 Nonlinear crystal

Nonlinear crystals can emit THz waves through optical rectification, which is a second-order nonlinear effect. It can be understood as a reverse process of electro-optic (EO) effect. When an intense femtosecond optical pulse passes through a nonlinear material, a static polarization is produced. The induced polarization is proportional to the envelope of the optical pulse. The time-dependent optical field results in the time-varying polarization, which acts as the source for THz radiation.

Since a second-order nonlinear effect only occurs in a noncentrosymmetric material, ZnTe, GaAs, GaP, InP, LiNbO₃, and LiTaO₃ are utilized to generate THz waves through optical rectification. In such a nonlinear process, phase matching [7] is a crucial factor in deciding the THz emission. The phase matching condition requires that the group velocity at optical frequencies matches the phase velocity at THz frequencies.

With appropriate choice of nonlinear crystal and wavelength of the optical pulse, this condition can be satisfied within a certain spectral regime. One of the most successful examples is ZnTe, which satisfies the criteria when 800 nm central wavelength optical pulses (Ti:sapphire laser) are available.

Some other crystals, such as LiNbO₃, have a larger EO coefficient than ZnTe does. However, there is a significant mismatch between the group velocity of optical pulses and the phase velocity of THz pulses in LiNbO₃ with a colinear geometry. To overcome the issue of mismatch but still benefit from the large EO coefficient of LiNbO₃, a method of tilting the optical pulse front was proposed by Hebling et al. [8–10]. Moreover, organic crystals (4-N,N-dimethylamino-4'-N'-methyl-stilbazolium tosylate (DAST), 4-N,N-dimethylamino-4'-N'-methyl-stilbazolium 2,4,6-trimethylbenzenesulfonate (DSTMS), and 2-(3-(4-hydroxy-tyryl)-5,5-dimethylcyclohex-2-enylidene)malononitrile (OH1)) that exhibit high EO coefficients have also been demonstrated as intense THz sources even though they are very delicate under intense optical excitation [11–14].

1.2.3 Gas

Compared with PCA or nonlinear crystal, gas is capable of emitting THz waves even if very intense optical pulses are applied. These optical pulses ionize the gas to form plasmas (electrons and ions), which radiates THz pulses. The ambient air is the most commonly used one in this type of THz sources.

There are various approaches to achieve THz wave generation from air plasma. In the first demonstration by Hamster et al. in 1993, optical pulses with a single frequency were used [15]. The THz radiation is attributed to the ponderomotive force-induced acceleration of electrons in the plasma [15,16]. Although the generation efficiency of this method is not great, the THz radiation can be scaled up by increasing the power of pump pulses without worry of causing damage to the source. More recently, the generation efficiency was proved to be several orders of magnitude higher when a two-color excitation technique was used [17]. Furthermore, water vapor was reported emitting strong THz waves by using this method as well [18]. The THz wave generation process in this scheme has been explained by a four-wave mixing model [17,19], a transient photocurrent model [20–22], or a full quantum model [23].

1.3 Liquid water as a source

It is noticeable that liquid sources were not mentioned in the last section. In fact, there is no demonstration of THz wave generation from liquids before 2017. Especially, liquid water has been historically considered as a “foe” in the THz community due to its significant absorption in the THz frequency range [24,25]. In contrast, people have successfully used liquid water to generate electromagnetic waves in other frequency regions for years.

Water is involved in a variety of physical and chemical processes on the earth. It exhibits complicated structures and abnormal properties in different conditions. For example, the temperature dependence of the density of water is not linear and the density rises to a peak at 3.98°C [26]. Besides, water has strong cohesion, adhesion, and surface tension. Thus, water can be used to form a thin film. Transparent, stable, nontoxic, and inodorous water is the ideal target in physics, biology, and chemistry. Considering its accessibility and plenty, water has the potential to be the low-cost source for various electromagnetic waves.

Water vapor was reported as a source (water maser) emitting microwaves at 22.0 GHz as early as 1986 [27]. Maser stands for “microwave amplification by stimulated emission of radiation”. The basic principle of maser is stimulated emission. Coherent radiation is produced by placing the amplifying medium into a resonant cavity. Maser-like stimulated emission has also been observed in nature from interstellar space. Such emission was observed

from water molecules in 1986 [27]. It was found that water molecules in star-forming regions could undergo a population inversion and emit radiation at about 22.0 GHz [28]. In 1994, water maser emission from X-ray-heated circumnuclear gas was reported by the same group [29].

The laser works in a similar principle as the maser does but produces coherent radiation with higher frequency (usually at visible or infrared wavelengths). Benefiting from the rapid development of laser technology, researchers are capable of studying interactions between high-intensity laser and matter. In recent years, supercontinuum emission and extreme ultraviolet (XUV) generation from liquid water through nonlinear processes have been successfully observed as well.

1.3.1 Supercontinuum generation from water

In 1970, supercontinuum generation was discovered by Alfano and Shapiro [30]. Supercontinuum generation is a process wherein laser lights with a narrow spectral bandwidth are converted into lights with a very broad spectral bandwidth. Supercontinuum is sometimes called white-light that usually refers to the radiation with spectra across 400–1100 nm. In 1987, the first observation of supercontinuum generation from water was reported [31]. When the incident laser pulse is of femtosecond duration, the spectrally broadened light emerges as a white disk surrounded by a rainbow-like pattern.

In 2003, experimental and theoretical results of white-light generation from the filamentation in water were presented [32]. A 1 kHz laser beam with the pulse energy of 2 mJ was used. The laser pulses were focused by a microscope objective into a water cell. The transmitted spectrum was collimated by an achromatic lens and imaged into the spectrometer.

The mechanisms for supercontinuum generation from water were fully discussed in Ref. [32]. Supercontinuum generation is the result of combined dynamic processes [32], such as self-focusing, group velocity dispersion (GVD), intensity clamping [33], self-steepening, anti-Stokes spectral broadening, filament fusion, filament breakup, and filament competition. Due to the nonlinear transformation of the laser pulse propagation in the water, the continuum spectrum of all frequencies arises.

In 2005, a systematical study of the influence of different parameters on the white-light generation was reported [34]. This study emphasized the focal position of the incident laser light within the medium and the pulse duration of the incident laser beam. Later, white-light generation with phase discontinuities and steeper intensity gradients was achieved with a 1-D spatial light modulator [35]. In 2016, the output supercontinuum spectra were extended to 2000 nm, by choosing a pump wavelength at 1860 nm [36]. No visible radiation was detected in this measurement.

1.3.2 XUV generation from water

XUV light has numerous applications in photoelectron spectroscopy and lithography [37]. Water has been found to be an efficient media to convert visible laser radiation into XUV [38,39], wherein high-order harmonic generation (HHG) from atoms and molecules is an established source for XUV radiation [40]. In 2003, HHG from water microdroplets was first reported [41].

In this nonlinear process, laser radiation is converted into integer multiples of its fundamental frequency up to very high orders. This phenomenon occurs when intense ultrashort laser pulses interact with a dielectric medium. Initially bound electrons are field ionized at particular phases of the laser electric field (close to its peak) and are driven away from their parent ions. Once the electric field of the laser pulse reverses, the electrons will decelerate on their outward-bound path and accelerate back toward their parent ions. Some of the ionized electrons will finally return to the ion core and recombine with the parent ions. During the time of recombination, the electrons generally possess nonzero kinetic energy. One photon per electron is emitted carrying the sum of the electron's kinetic energy plus the ionization potential.

A glass capillary was mounted inside a vacuum chamber and the water droplet jet was aimed vertically downwards. A piezo element was used to control the droplet's repetition rate. Optical pulses interact with the water droplet to induce HHG.

1.3.3 X-ray generation from water

With the development of femtosecond lasers, laser induced plasma for X-ray generation attracts considerable attentions due to its small size, high brightness, and high spatial stability. The conventional targets for X-ray generation were limited to metals and gases. Since 1993, some reports occurred by using a liquid target such as fluoride, ethanol, water, and so on [42–45]. The main purpose is to solve the problem caused by debris and to achieve a continuous operation.

Liquid is able to provide a high-density plasma and electrons with keV energy. Generally, X-ray emission spectra from liquid reflect two processes of deaccelerating electrons. A continuous, broadband X-ray is emitted by the collision of the accelerated electrons with the atomic nuclei of the target. The characteristic radiation at a certain wavelength is resulted from the process that electrons from higher energy level filling the vacancies left by the electrons of the inner shell.

1.4 Challenges and opportunities

As discussed in the previous section, water has been used to emit electromagnetic waves from X-ray to infrared

waves under the excitation of intense laser pulses. A similar approach of focusing intense optical pulses to excite water may also work for the generation of THz waves.

However, there are more challenges in obtaining THz radiation from water. The first problem leading the impediment is that liquid water has strong absorption characteristics in the THz frequency regime. Its power absorption at THz frequencies was measured by Ronne et al. in 1997 [24]. The power absorption coefficient of 220 cm^{-1} at 1 THz means only one photon at 1 THz can go through 1 mm thick water layer with 3.6×10^9 THz photons entered at room temperature. Thus, THz signals may be completely buried in the absorption even if THz radiation has already been generated from water. Moreover, the detailed research of laser-induced breakdown and ionization process in water for THz wave generation have not been well studied. Optimal conditions need to be experimentally tested. Refraction and total internal reflection caused by the interfaces between water and air make the situation more complicated.

Opportunities can also be seen in the terahertz aqueous photonics. Compared with air, liquid water has a lower ionization threshold but a higher molecular density [46–49], which indicates that under the identical excitation liquid water can provide more electrons and ions in the same unit volume. Unlike PCA and nonlinear crystals that suffered from permanent damage under the excitation of intense laser pulses [12,50,51], liquid water can quickly replenish itself due to its fluidity. Hence, liquid water has the potential to be developed as a THz source to meet desired applications. In addition, THz waves generated from liquid water will be closely related to laser-induced ionization process in water. Therefore, terahertz aqueous photonics could provide more in-depth information on laser-water interaction.

2 Terahertz wave generation from a water film

2.1 Free-flowing thin water film

Bulk liquid water is a strong absorber in the THz frequency range, making liquid water has historically been sworn off as a THz source. To mitigate the considerable loss of THz waves, the water with much less than 1 mm thickness is an intuitive choice to study THz wave generation.

Gravity-driven, free-flowing water films have been efficaciously used owing to their simple design and almost unmatched ability to generate a thin, continuous, and stable film of liquid water in free space [1]. The gravity-assisted flow along two metal wires forms the water film. The thickness of the water film is adjusted by the height difference between an upper reservoir and the top of the

wires mounted in an aluminum frame. The system is circulated by a peristaltic pump.

By using the concept of water flowing along wires, a similar water film system was built. These wires have a diameter of $170\ \mu\text{m}$, and are separated by $4\ \text{mm}$. Under the effect of water's surface tension, the water goes along the wires and forms a water film as shown in Fig. 2. Unlike the case in Ref. [1], the thickness of this water film was adjusted by throttling the water flow rate. An optical second-harmonic intensity autocorrelator was used to measure and calibrate the thickness of the water film. The corresponding result is plotted in Fig. 3, which shows a linear relationship between the thickness of the water film and the flow rate. In this system, the thickness of the water film can be varied from 50 to $330\ \mu\text{m}$.

2.2 Experimental set-up

Figure 4 schematically shows the experimental set-up for



Fig. 2 Photo of the water film. Two aluminum wires are separated by $4\ \text{mm}$. The thickness of the water film is controlled by the water flow rate

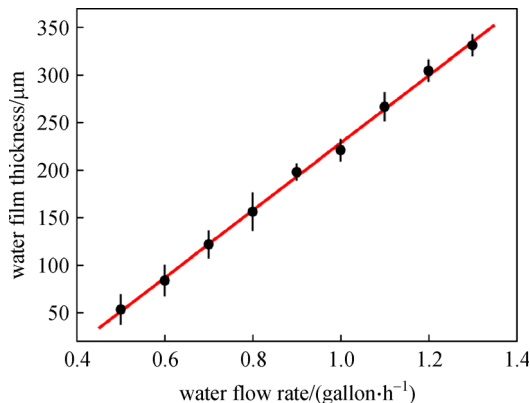


Fig. 3 Thickness of the water film versus the water flow rate

the generation of THz waves. An amplifier laser (Ti:sapphire) with $800\ \text{nm}$ central wavelength and $1\ \text{kHz}$ repetition rate was used. An optical polarizer was placed to assure the p-polarized optical beam. The following half-wave plate (HWP) further adjusted the polarization of the optical beam. The laser pulse duration was adjusted by moving the compressor stage integrated within the laser. The original pulse duration was $58\ \text{fs}$. The incident angle of the laser beam on the water film was tilted to 25° from the normal to reduce the water sputtering onto the surface of optics. The thickness of the water film was set to be $177\ \mu\text{m}$. The laser beam was focused into the water film by a 1-inch effective focal length parabolic mirror, forming a plasma inside the water film. Filters were placed to block the remaining laser beam as well as any white light simultaneously generated from the water film in addition to the THz radiation. A tungsten wire-grid polarizer was applied as the THz polarizer. Standard electro-optic sampling (EOS) [52] with a $3\ \text{mm}$ thick $\langle 110 \rangle$ -cut ZnTe was used to detect the THz electric field with a cutoff frequency around $2.5\ \text{THz}$. The flow velocity of the water is about $1.3\ \text{m/s}$, meaning that the water film flows about $1.3\ \text{mm}$ between two laser pulses. This distance is much greater than the diameter of the focal spot of the laser beam, which indicates that each THz pulse will not be affected by previous interaction between the water and laser pulses.

2.3 Terahertz radiation from a water film

By using the above experimental set-up, THz wave generation from a water film is achieved. The THz waveform is shown as curve B in Fig. 5(a) [53]. Since EOS provides coherent signals, the obtained THz radiation is obviously not just a tail of black-body radiation. To confirm that the THz radiation is mainly emitted from the water film rather than the air plasma, the water film is translated along the direction of laser propagation. The schema of relative positions between the water film and the plasma is shown on the left-hand side of Fig. 5(a). The corresponding THz waveforms are plotted on the converse side of Fig. 5(a). For curve A, the focal point of the laser is behind the film: the laser beam passes through the water and is focused to generate THz waves from an air plasma. For curve B, the focal point is near the center of the water film: a plasma is formed inside the water film, and the THz field emitted from liquid water is measured. For curve C, the laser beam is focused and forms an air plasma before the water film. Little THz radiation is detected due to the strong absorption of the water film. It is noticeable that the THz signals from air plasma will be clearly observed if the thickness of the water film is reduced to $100\ \mu\text{m}$ or less. Curve D is shown as a reference: no water film is present and only the THz wave generated from air plasma is detected.

By scanning the water film along the optical axis,

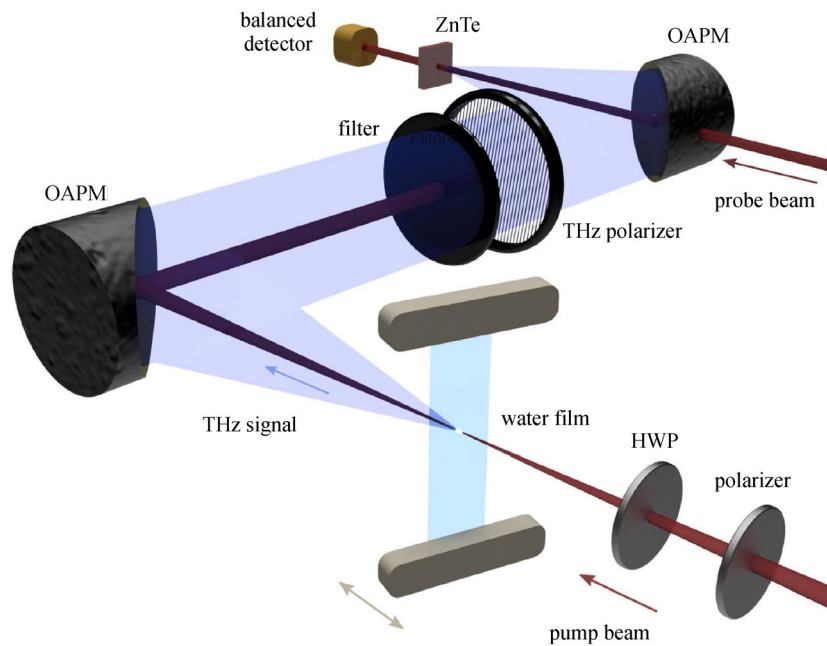


Fig. 4 Experimental set-up for THz wave generation from a water film. Broadband THz wave is generated by tightly focusing the laser beam into a gravity-driven wire-guided free-flowing water film [53]. The water film can be moved in the laser propagation direction by a mechanical translation stage. OAPM, off-axis parabolic mirror. HWP, half-wave plate

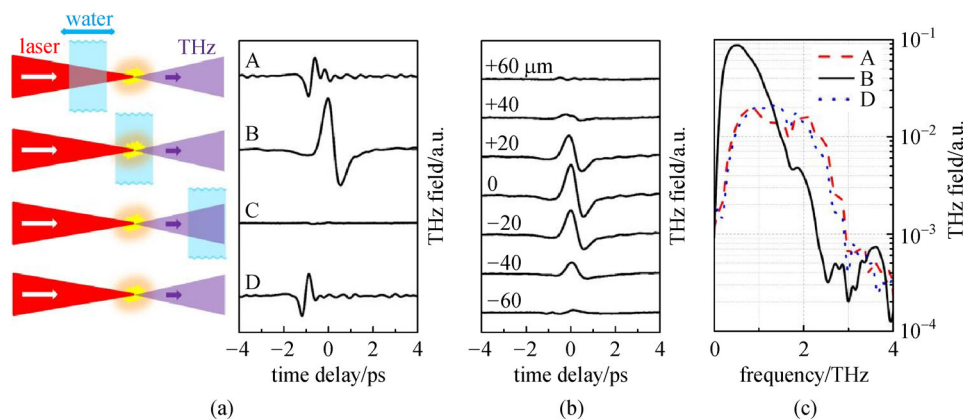


Fig. 5 Measurements of the THz fields when the water film is translated along the direction of laser propagation [53]. (a) THz waveforms are plotted from curve A to curve C when the water film is before, near, and after the focus, respectively; curve B shows the THz waveform generated from liquid water; curve D is the reference with no water film. Yellow spark and bluish pane represent the plasma and the water film respectively. THz emission angle shown in the figure is not meant to be indicative of actual THz emission pattern. (b) THz waveforms when the water film is moved near the focal point. The 0 position is set to the place with the strongest THz field. Relative positions are listed with the corresponding waveforms. The negative sign means the water film is located after the focal point. The positive sign indicates the opposite case. (c) Comparison between the THz field from water and that from air plasma in the frequency domain. The dashed, solid, and dotted spectra correspond to curve A, curve B, and curve D in (a), respectively. The laser pulse is temporally stretched to 550 fs for these measurements

THz radiation from different sources can be clearly differentiated. The timing distinctions of the waveforms in Fig. 5(a) are indicative of different generation sources. A time delay is observed from the THz waveform from liquid water compared with other generations. Figure 5(b) shows

the measurements of THz waveforms as the water film is tracked along the direction of laser propagation marking a relative position across -60 to $+60$ μm . The measurement shows that the emitted THz waves are significantly sensitive to the relative position between the water film

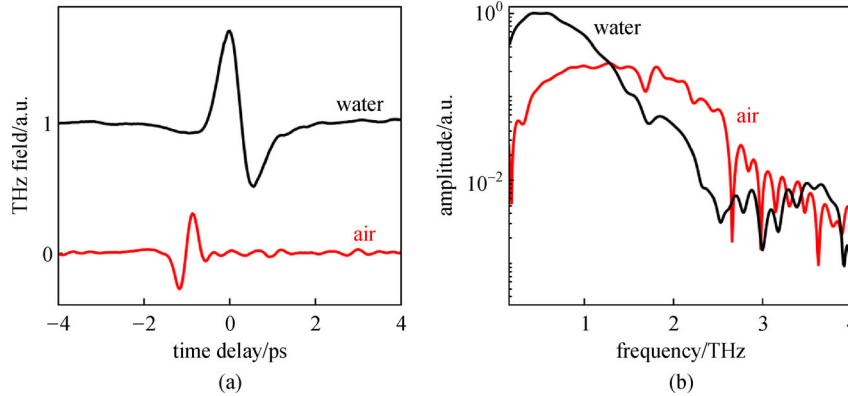


Fig. 6 Comparison of THz waves generated from water and air in the (a) time domain and (b) frequency domain

and the focus. The THz radiation can be detected only within a roughly 60 μm scanning range of the water film. It should be mentioned that no THz radiation is detectable when only part of the plasma is located outside the range of the water film. The plasma located on the interface does not give a spurious THz signal.

2.4 Comparison between terahertz radiation from water and air

Ambient air is one of the most extensively used THz sources. It is necessary to compare the THz radiation generated from water and air in the same experimental condition. Actually, curve B and curve D in Fig. 5 offer a reasonable comparison. To make it clear, only these two signals are plotted in Fig. 6. Figure 6(a) depicts that the THz field from the water film is 1.8-times stronger than that from the air. The corresponding comparison in the frequency domain is shown in Fig. 6(b). Note that the feature around 1.7 THz is caused by the water vapor absorption. The measured THz radiation from the water has more low-frequency components and less high-frequency components with a peak at 0.5 THz. In addition, the bandwidth is narrower than the signal from air plasma. Their difference in the frequency domain may result from the fact that liquid water absorbs more high-frequency components than low-frequency components in the THz frequency region [1]. It should be mentioned that the result in Fig. 6 only shows the comparison in this experimental condition. The signal from liquid water will be rather stronger if other optimal conditions (the incident angle of the laser beam on the water film, the thickness of the water film, the detection angle, etc.) are satisfied, which will be discussed in later sections.

2.5 Effect of optical polarization and pulse energy

Polarization and pulse energy of the optical beam are two important parameters that may affect THz wave generation from liquid water.

The relationship between the THz radiation and the optical polarization is exposed by measuring the THz fields generated from the optical excitation beams with different polarizations. Since the water-air interface reflects more s-polarized THz waves according to the Fresnel equations, the p-polarized component of the THz field is studied here. A wire-grid THz polarizer was applied for the measurement. The polarization of the optical beam was controlled by the HWP in the optical path (see Fig. 4). The corresponding result is shown in Fig. 7. 0° refers to the p-polarized optical beam and 90° refers to the optical beam with s-polarization. It is shown that strong THz radiation is achieved with a p-polarized optical beam, while an s-polarized optical beam offers a sparse contribution. One possible explanation is that the polarization of the THz field is dependent on the optical polarization, as the measured p-polarized component of the THz field has a cosine squared relationship with the angle of the optical polarization. Also, the different Fresnel loss of the optical beam caused by the air-water interface with different polarization will change the laser intensity inside the water film, thus, lead to the variation of THz radiation. A similar

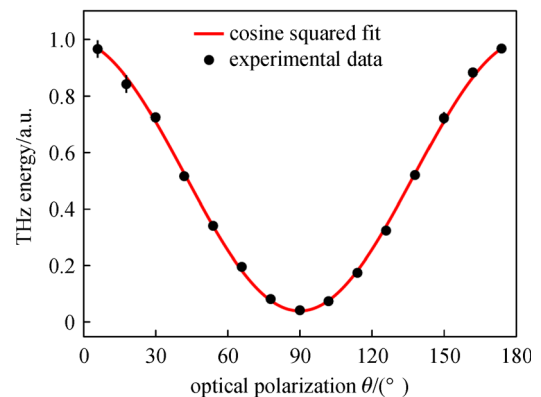


Fig. 7 Energy of p-polarized THz field from liquid water with different linearly optical polarization. 0° and 90° refer to p-polarized and s-polarized optical beam respectively [53]

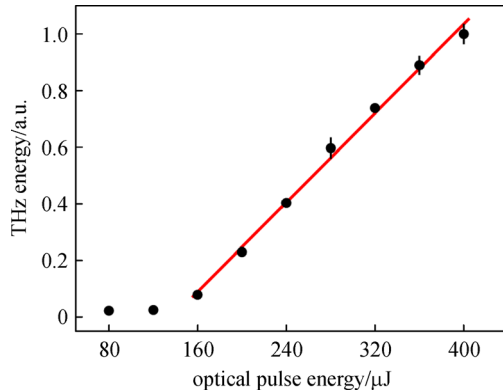


Fig. 8 Normalized THz energy from liquid water as a function of incident optical pulse energy [53]. The water film will be broken if the energy of the excitation pulse is over 420 μJ

phenomenon was reported in Ref. [54] wherein a particle-in-cell model [55] was applied to simulate the observation. This result goes against the case of THz wave generation from one-color laser-induced air plasma. It is well known that the THz radiation from air plasma with one-color optical excitation does not depend upon the polarization of the optical beam [15,16], which means that the THz energy keeps constant with various optical polarizations.

Furthermore, the linear energy dependence observed in Fig. 8 is different from the quadratic relation in the case of THz wave generation from the one-color laser-induced air plasma [56]. Figure 8 also shows a laser excitation threshold at about 160 μJ for the detectable THz field from liquid water under this experimental condition. The 177 μm thick water film will be broken if the energy of the excitation pulse is over 420 μJ . This rupture may be caused by the occurrence of shock waves, plasma expansion, and water ejection when high-intensity laser pulses are focused into liquid water [57–61]. These effects weaken the stability of the water film as laser energy is increased.

2.6 Effect of water film's thickness

The wire-guided free-flowing water film's thickness can be easily controlled by throttling the flow rate, which facilitates the study of how the water film's thickness impacts on the THz radiation. THz waveforms generated from water films with different thicknesses are plotted in Fig. 9.

To make sure that the water film was not broken under the excitation of intense laser pulses, the thickness of the water film was set to be greater than 130 μm in this measurement. Figure 9 shows that the peak of the THz waveform linearly shifts in time with various thicknesses. This time shift comes from the path difference of THz waves in water with difference thickness. The central frequency of the THz radiation is around 0.5 THz in this case (see Figs. 5(c) and 6). From the linear fitting (red dash

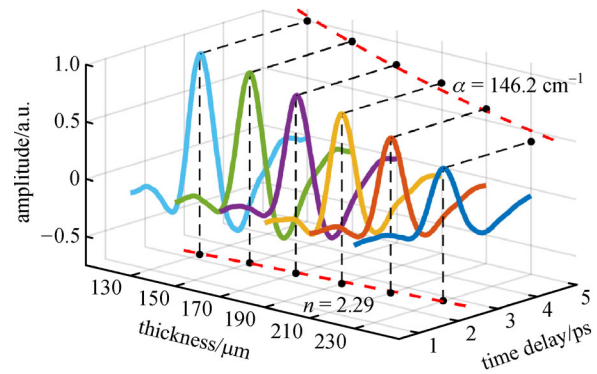


Fig. 9 THz wave generation from water films with different thicknesses. The refractive index of water at 0.5 THz is calculated to be 2.29 from the time shift of the THz field. The absorption coefficient of water at 0.5 THz is calculated to be 146.2 cm^{-1} from the attenuation of the THz field's amplitude

line), the refractive index of water at 0.5 THz can be calculated as $n_{\text{THz}} = 2.29$ if increasing the thickness of the water film is assumed to go symmetrically with respect to the center of the film. Furthermore, the attenuation of the THz field amplitude with the increased thickness is observed in Fig. 9. The attenuation of amplitude results from the increasing absorption of a thicker water film. From the exponential fitting (red dash curve), the absorption coefficient of water at 0.5 THz is calculated to be 146.2 cm^{-1} . The calculated refractive index and absorption coefficient are very close to the values found in previous work: $n_{\text{THz}} = 2.27$ and $\alpha = 150 \text{ cm}^{-1}$ [1]. It is noteworthy that only the thickness of the water film was changed, and no further optimization was applied in this measurement.

2.7 Forced-flowing thin water film

THz wave generation from a gravity-driven free-flowing water film has already been demonstrated. However, it is observed that the film will be broken if the laser intensity is too high, which may impede the development of intense liquid sources for THz waves. To solve this problem, a nozzle jet was utilized to produce a forced-flowing water film to bear intense laser pulse. A liquid jet with a pressure of 30 psi was used to create a 5 mm wide, 120 μm thick water film, as shown in Fig. 10.

By using this forced-flowing water film, the laser pulse energy can be greatly increased without worrying about the occurrence of rupture, which assures that a plot of energy dependence with a large range can be seen. Similar to Fig. 8, Fig. 11 also shows that the THz energy linearly increases with the optical pulse energy (up to 2 mJ). No saturation is observed within this range as well. This result is indicative of a way to realize intense THz radiation from water: using intense laser pulses for excitation.



Fig. 10 Photo of a 120 μm thick water film formed by a water jet with a flat nozzle [62]. The laser beam is focused into the center of the film where is flat and stable

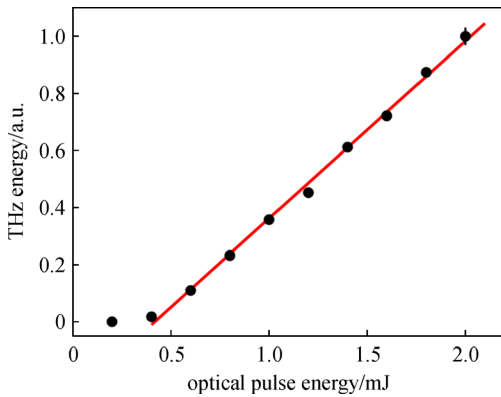


Fig. 11 Normalized THz energy as a function of the optical pulse energy [62]. The red line shows a linear fit

2.8 Mechanism of generation process

With these experimental observations, the physical mechanism of THz wave generation from water can be analyzed. Laser-induced plasma formation associated with a dipole radiation model is proposed to explain the generation process.

Figure 12 [62] is a cross-section diagram of the

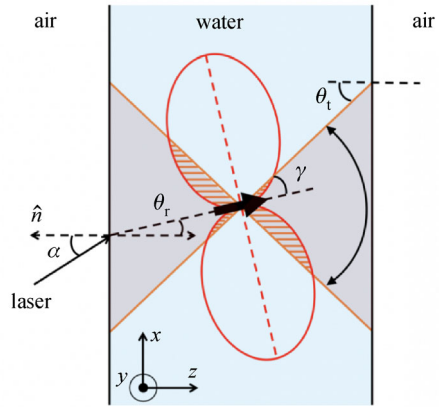


Fig. 12 2D cross-section of the THz wave generation process in a water film [62]. Intense pulses ionize water at the focal point in the direction of the refracted laser beam. The angle of incidence on the air-water interface is α . The black arrow shows the dipole orientation direction. Due to the total internal reflection at the water-air interface, THz emission at 0.5 THz can be coupled out only when $-24.6^\circ < \theta_e < +24.6^\circ$

generation process in a water film. Intense laser pulses ionize water molecules through multi-photon ionization (MPI) [63–67], tunneling ionization (TI) [68,69], and cascade ionization (avalanche ionization) [64,65,70–73] in the focal volume. Plasmas (electrons and ions) are formed in the ionized area. The quasi-free electrons (will be called as free electrons in later sections for simplicity) in water [74] experience the ponderomotive force and move toward the areas of lower electron density due to the density-gradient distribution. Simultaneously, other ionized particles are relatively stationary due to their large masses. Since the electrons move slower than the envelope of the laser pulse, the density of the ionized carriers always keeps identical in the forward direction. As a result, electrons are accelerated backward and create a dipole oriented along the laser propagation direction [15,16], which emits electromagnetic waves including THz frequencies. Reflection of the optical beam at the air-water interface and refraction of the THz beam at the water-air interface are considered. THz beams that experience multiple reflections between the interfaces are ignored due to the strong absorption of water.

2.8.1 Laser-induced plasma formation

Electrons are produced through MPI/TI and cascade ionization at the focus. MPI/TI directly ionizes water molecules while cascade ionization desires the presence of free electrons for initiation. These free electrons come from the background electrons and MPI/TI.

Free electrons absorb photons to gain energy from laser pulses through collision with surrounding atoms or molecules, which is known as inverse bremsstrahlung

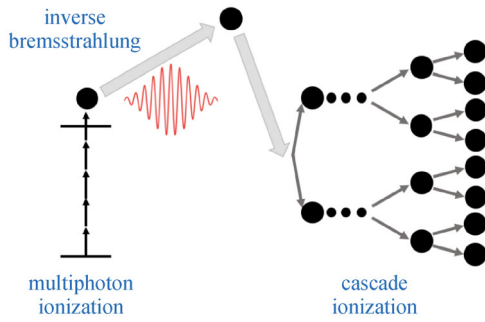


Fig. 13 Visualization diagram of laser-induced plasma formation

absorption. Water can be treated as an amorphous semiconductor with a bandgap of $E_g = 6.5$ eV [48,49,75,76]. Once achieving the energy greater than the ionization energy E_g , a free electron will be produced. This results in two free electrons of lower energy, which in turn absorb energy from the laser and ionize two more electrons, and so on. Thus, the process leads to a cascade of electrons. Figure 13 shows the process of plasma formation. It needs to be mentioned that TI occurs or dominates over MPI when the laser intensity is sufficiently high to decrease the potential barrier allowing electrons to escape. The Keldysh parameter γ is widely used to indicate which process is dominant.

$$\gamma = \sqrt{E_g/U_p}, \quad (1)$$

where U_p is the laser ponderomotive potential energy. $\gamma > 1$ implies MPI while $\gamma < 1$ indicates TI.

Assuming the laser pulse propagates in the z -direction, the electric field envelope $E(z, r, t)$ follows [77]:

$$\begin{aligned} \frac{\partial E}{\partial z} = & \frac{i}{2nk_0} \nabla_T^2 E + ik_0 n_2 |E|^2 E - \frac{i\beta_2}{2} \frac{\partial^2 E}{\partial t^2} \\ & - \frac{\sigma}{2} (1 + i\omega\tau) \rho E - \frac{\beta^{(k)}}{2} |E|^{2K-2} E. \end{aligned} \quad (2)$$

The terms on the right-hand side represent transverse beam diffraction, nonlinear self-focusing, group velocity dispersion (GVD), plasma absorption and defocusing, and multiphoton absorption, respectively. Here, n is the refractive index, k_0 is the wave vector, n_2 is the nonlinear coefficient, β_2 represents GVD, $\sigma = (ke^2\tau/(m\omega\epsilon_0))/(1 + \omega^2\tau^2)$ is the cross-section for inverse bremsstrahlung absorption [78], ω is the optical frequency, τ is the electron collision time, and $\beta^{(k)}$ is the nonlinear coefficient for K -photon absorption. The last term need be modified to $w(\rho_{\text{water}} - \rho)E_g E/(2I)$ when TI dominates [79]. w is the ionization rate, ρ_{water} is the water molecular density, and I is the laser intensity. The electron density $\rho(z, r, t)$ satisfies the rate equation [74]:

$$\frac{\partial \rho}{\partial t} = \left(\frac{\partial \rho}{\partial t} \right)_{\text{mp}} + \eta_{\text{cas}} \rho - \eta_{\text{diff}} \rho - \eta_{\text{rec}} \rho^2. \quad (3)$$

The first two terms on the right-hand side correspond to the generation of electrons from MPI $\left(\left(\frac{\partial \rho}{\partial t} \right)_{\text{mp}} \right)$ and cascade ionization ($\eta_{\text{cas}} \rho$). The first term becomes $w(\rho_{\text{water}} - \rho)$ in the case of TI. The other two terms in Eq. (3) describe the loss of electrons from diffusion ($-\eta_{\text{diff}} \rho$) and recombination ($-\eta_{\text{rec}} \rho^2$). The laser pulse is considered to have a Gaussian profile with its intensity as follows:

$$I(t) = 0.94 \frac{\varepsilon_p}{\tau_p} \exp \left[-4 \ln 2 \left(\frac{t}{\tau_p} \right)^2 \right] / (0.5\pi\omega_0^2), \quad (4)$$

where ε_p is the laser pulse energy, τ_p is the laser pulse duration, and ω_0 is the beam waist at the focus.

In condensed media, Keldysh [68] derived an approximate expression for the multiphoton ionization rate as [48,74]

$$\begin{aligned} \left(\frac{\partial \rho}{\partial t} \right)_{\text{mp}} \approx & \frac{2\omega}{9\pi} \left(\frac{m\omega^2}{2\hbar\omega} \right)^{1.5} \left(\frac{e^2}{8mE_g\omega^2 c\epsilon_0 n} I \right)^K \\ & + \exp(2K) \Phi \left(\sqrt{2K - \frac{2E_g}{\hbar\omega}} \right), \end{aligned} \quad (5)$$

with $\Phi(x) = \exp(-x^2) \int_0^x y^2 dy$.

In the case of TI, the ionization rate can be calculated by Ammosov-Delone-Krainov (ADK) model [69]:

$$w(t) = 4\omega_a \frac{E_a}{|E|} \exp \left(-\frac{2E_a}{3|E|} \right). \quad (6)$$

The cascade ionization rate is given by [48,74]

$$\eta_{\text{cas}} = \frac{\sigma}{n^2 E_g} I - \frac{m\omega^2 \tau}{M(1 + \omega^2 \tau^2)}, \quad (7)$$

where M is the mass of a water molecule. The first term on the right-hand side results from the inverse bremsstrahlung absorption [74,77]. The second term relates to the energy transfer from the electrons to heavy molecules [74,78].

2.8.2 Dipole radiation model

The ionized electrons are accelerated to form a dipole in the direction of the refracted laser beam that emits THz radiation as shown in Fig. 12. To confirm the applicability of the dipole radiation model, the following experiments were conducted. The laser pulses with horizontal polarization, 800 nm central wavelength, and 1 kHz repetition rate were delivered from a Ti: sapphire amplified laser. It was focused into a 120 μm thick water film by a 2-inch

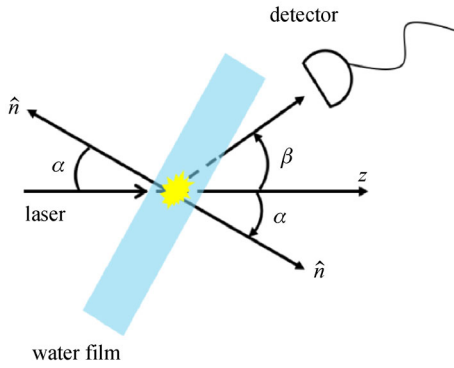


Fig. 14 Illustration of incident angle α and angle of detection β [62]. All angles are defined with respect to the z -axis

effective focal length lens (F/4) ionizing water molecules at the focus. A 2 mm thick $\langle 110 \rangle$ -cut ZnTe crystal configured for EOS [52] and a commercially available Golay cell were both used for the detection of THz waves. An illustration of the incident angle α for the laser beam and the angle of detection β for the detector is shown in Fig. 14 [62]. These two angles are both defined with respect to the laser propagation direction (z -axis) and can be changed by rotating the film and detector, respectively. \hat{n} is the surface normal of the water film. The sign of the angle is negative/positive when it is measured clockwise/counter-clockwise from the z -axis. The optical pulse duration is tuned to be 300 fs for maximizing the THz signal with the 120 μm thick water film.

Figure 15 [62] plots the THz waveforms generated from the water film with two opposite angles of incidence ($\alpha = \pm 65^\circ$) and detected in the laser propagation direction. The corresponding spectra are shown in the inset. The central wavelength and full width at the half maximum (FWHM) are both about 0.5 THz. Therefore, the parameters (index

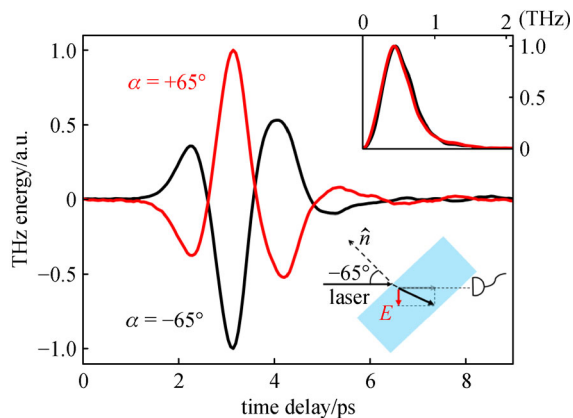


Fig. 15 THz waveforms generated from a water film with opposite angles of incidence ($\alpha = \pm 65^\circ$) [62]. The corresponding spectra and dipole approximation illustration are shown in the insets

of refraction and absorption coefficient) at 0.5 THz [1] are used in the following calculation and simulation. As show in Fig. 15, the waveform keeps its amplitude but completely flips over when the angle of incidence changes its sign. This observation applies to all opposite angles of incidence. It can be inferred that the dipole orientation is along the propagation direction of the refracted laser beam, illustrated as a black arrow in Fig. 15. The projected signal from the dipole reverses in direction when the angle of incidence changes the sign, which accounts for the flipped waveforms.

2.9 Radiation pattern

In the last section, a dipole model was proposed to explain the mechanism of THz wave generation from liquid water. Similar to the case in air, a spatial net charge distribution created by the ponderomotive force acts like a Hertzian dipole and radiates THz waves [15,16]. However, the existence of the interfaces makes the scenario more complicated. Specifically, the refraction of the laser beam induced by the first interface (air-water) changes the orientation of the dipole while the total internal reflection and refraction of the THz beam caused by the second interface (water-air) significantly affect the radiation angle of THz waves. The model also predicts that backward THz radiation should be present even though only the forward radiation has been paid attention in the previous study. Thus, simulations and measurements of the THz radiation pattern can be very useful to further verify the dipole radiation model.

At the air-water interface, refractive angle $\theta_r(\alpha)$ and transmittance $T_1(\alpha)$ for a given α is obtained according to Snell's law and the Fresnel equations, which are determined by the refractive indices of the 800 nm optical beam in air and water. The maximum $\theta_r(\alpha)$ is 48.8° when $\alpha = 90^\circ$. THz waves radiated by the dipole propagating in the water film are attenuated due to the absorption of water. If the thickness of the water film is d , the absorption in the different direction $\theta_t(\beta)$ from the source can be described as $\exp[-\alpha_{\text{THz}}d/(2\cos\theta_t(\beta))]$, where α_{THz} is the power absorption coefficient of water. Multiple reflections of THz waves are neglected in the calculation due to the strong absorption of water. Additionally, the dipole radiation energy is proportional to $\sin^2(\gamma)$, where $\gamma(\alpha, \beta) = \theta_t(\beta) - \theta_r(\alpha)$ is the angle measured with respect to the dipole direction. Finally, the THz waves are detected after passing through the water-air interface with a transmittance $T_2(\beta)$. To sum up, the angular dependence of THz energy on α and β is described as [62]

$$I_{\text{THz}}(\alpha, \beta) \propto T_1(\alpha)T_2(\beta)\sin^2[\gamma(\alpha, \beta)]\exp\left(-\frac{\alpha d}{2\cos\theta_t(\beta)}\right). \quad (8)$$

Figure 16 [62] plots the simulation result of the

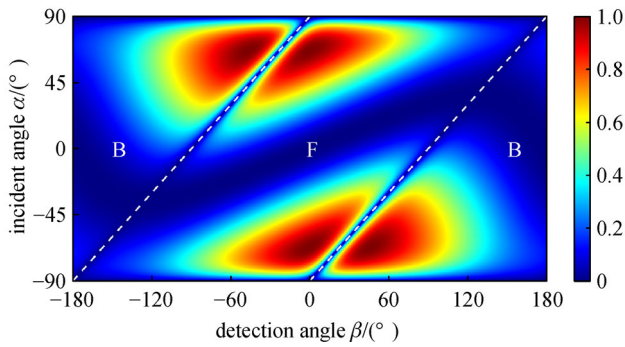


Fig. 16 Simulation result of normalized THz energy $I_{\text{THz}}(\alpha, \beta)$ using the dipole radiation model [62]. The dashed lines indicate the cases of $|\alpha - \beta| = 90^\circ$, which means the detector is located in the plane of the water film. These dash lines separate the plots into three parts, labeled as “B”, “F”, and “B”. “B” and “F” indicate backward and forward propagating THz signal, respectively

normalized THz energy $I_{\text{THz}}(\alpha, \beta)$. A micro-plasma is created in the water film with the tightly focused geometry [56]. This plasma can be considered as a point source emitting THz waves in all directions. Thus, besides the forward (F) propagating signal, the signal propagating in the backward (B) direction is also expected. These two parts are separated by the dashed line in the plot and labeled separately. Due to the symmetric geometry of the model, the energy distribution pattern for forward and backward propagating THz signals are the same when the plasma is located at the center of the water film. The dashed lines also indicate the case of $|\alpha - \beta| = 90^\circ$, which means that the detector is put in the plane of the water film. When $|\alpha - \beta| > 90^\circ$, the THz waves propagate in the backward direction.

To verify the simulation result, the THz signal versus α was measured when β was fixed at 0° or 55° , both EOS and a Golay cell were used for the detection in the measurement. The corresponding results are plotted in Fig. 17 [62].

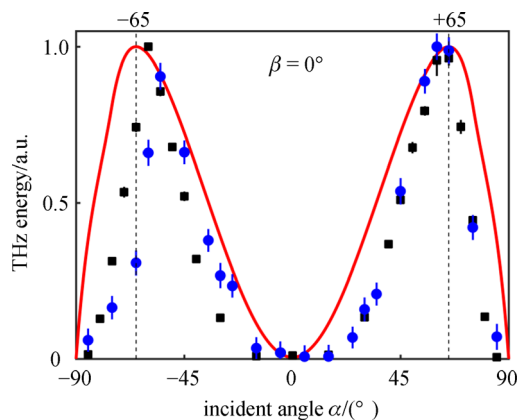


Fig. 17 THz energy versus the angle of incidence α with $\beta = 0^\circ$ [62]. The black squares are the data measured by EOS and the blue dots are measured by a Golay cell. Only forward propagating signals can be detected for $\beta = 0^\circ$

The red solid line shows the simulation result. The EOS result (black squares) is obtained from the temporal integration of the whole THz waveform. The result from the Golay cell is plotted as the blue dots. As shown in the plot, the optimal incident angle of the laser beam is 65° , which results from the dipole’s orientation. The coincidence of the experimental data and the simulation exhibits the validity of the dipole radiation model. Note that only the forward THz waves can be measured when $\beta = 0^\circ$. In addition, the calculation with $\alpha = 65^\circ$ indicates that 80% of the THz energy dissipates due to the total internal reflection at the water-air interface and the strong absorption of water.

Even though EOS generally offers a better signal-to-noise ratio, its optical alignment for the detection of radiation pattern is complicated. By contrast, a Golay cell is capable of measuring radiation pattern including both forward and backward directions easily. Thus, the Golay cell is used for the case of $\beta = 55^\circ$ (Fig. 18) [62]. In this case, the signal comes from the backward radiation THz waves is observed when $-90^\circ < \alpha < -35^\circ$. The detectable backward propagating THz signal supports the dipole radiation model. Compared to the simulation result (solid line), stronger signals are measured in the forward direction. This may be a consequence of plasma deviation from the center of the film.

2.10 Effect of optical pulse duration

It has reported that long pulse helps enhance X-ray generation from a liquid plasma [79]. To study the dependence of the THz radiation on the optical pulse duration, the laser pulse was stretched in time to achieve different pulse duration. Figure 19 shows the normalized THz energy from water and air plasma versus the optical pulse duration. The THz energy from water or air plasma is normalized to the corresponding maximum respectively.

The optical pulse duration is at its minimum of 58 fs

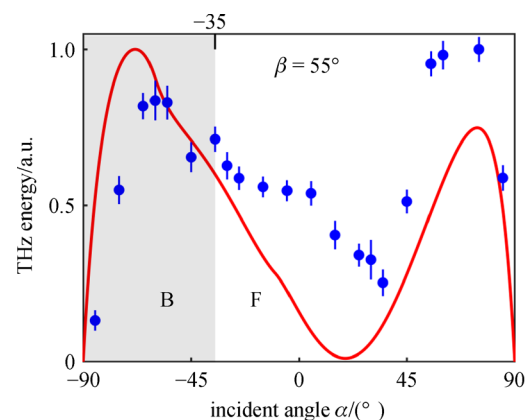


Fig. 18 THz energy versus the angle of incidence α with $\beta = 55^\circ$ [62]. The blue dots are measured by a Golay cell. Backward propagating signals are detected for $-90^\circ < \alpha < -35^\circ$

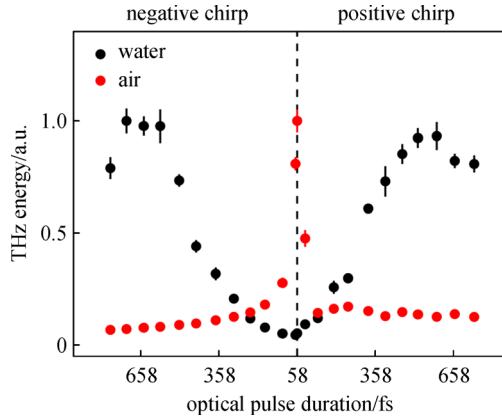


Fig. 19 Normalized THz energy from liquid water and air plasma with different pulse duration of the laser beam [53]. Black squares represent the THz energy from liquid water and red dots represent the case of air plasma. The optical pulse duration is at its minimum of 58 fs when no frequency chirp is applied. On the left-hand side of the figure, negative chirps are applied to increase the optical pulse duration while the case of positive chirps is shown on the right-hand side of the figure. The energy of the laser pulse is 0.4 mJ for these measurements

when no chirp is applied. The left-hand side of Fig. 19 shows the case of negative chirps, where the low-frequency component of the pulse lags the high-frequency component. Positive chirps indicate the opposite and the corresponding measurements are shown on the right-hand side of Fig. 19.

Unlike the THz radiation from air plasma, where the signal is maximized at a minimum pulse duration with no additional chirp, liquid water generates a maximum field at a longer pulse duration. Furthermore, by comparing the left part and the right part of Fig. 19, it is shown that the frequency chirp of the optical beam is not a dominant factor compared with the contribution from the pulse duration. This can also be supported by Fig. 20, which plots the similar spectra of THz radiation by using the same optical pulse duration but opposite chirps. For simplicity, only positive chirps will be applied in future investigation.

The above observations may result from the dependence of plasma formation in water upon the optical pulse duration. To confirm the assumption, further experiments and simulations are indispensable. More in-depth discussions will be shown later.

3 Terahertz radiation from liquid water under two-color excitation scheme

3.1 Glory of two-color excitation scheme in gases

THz wave generation through the tunneling ionization process in gases induced by two-color (fundamental frequency ω and its second-harmonic 2ω) femtosecond

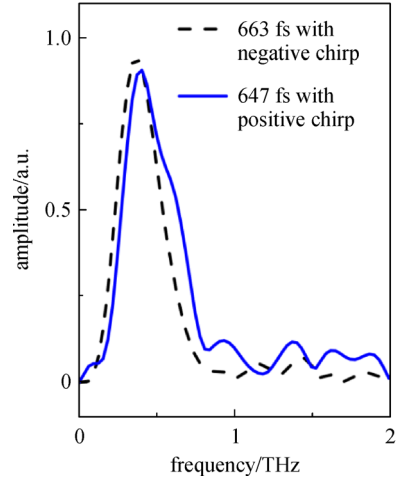


Fig. 20 Spectra of THz radiation generated from the water film with a negative chirped 663 fs pulse and that with a positive chirped 647 fs pulse

laser pulses [17,80] is a significant milestone in the THz community due to its impressive intensity, remarkably broad bandwidth, and applications in nonlinear interactions and THz spectroscopy [81–83]. There is no exaggeration to say that THz wave generation under the two-color excitation scheme has been always one of the most popular topics since it was reported by Cook and Hochstrasser in 2000 [17]. A typical schematic diagram is shown in Fig. 21. An intense femtosecond laser pulse ω and its second harmonic 2ω are focused into the air to generate air plasma for the emission of THz waves. Commonly, the 2ω laser pulse is generated by applying a type-I β -barium borate (BBO) crystal to the ω laser pulse. The output THz radiation is controlled by the phase delay between ω pulse and 2ω pulse. Compared with using only ω pulses for the excitation, the mixing of ω and 2ω pulses has shown to provide enhancement of THz wave generation efficiency by several orders of magnitude [17].

The generation mechanism of the two-color excitation

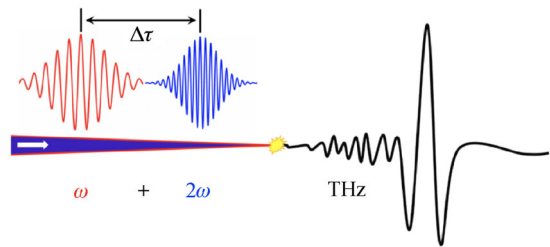


Fig. 21 Schematic diagram of THz wave generation from a two-color laser pulses induced air plasma. An intense femtosecond laser beam ω and its second harmonic 2ω are focused to generate plasma in the air. In the most common way, a β -BBO crystal is applied for the generation of 2ω pulse. The output THz waves are determined by the phase delay between ω pulse and 2ω pulse

scheme was phenomenologically assigned to a four-wave-mixing model as

$$E_{\text{THz}}(t) \propto \chi^{(3)} E_{2\omega}(t) E_{\omega}^*(t) E_{\omega}^*(t) \cos\phi, \quad (9)$$

where E is the field amplitude of the frequency components specified by the subscript, $\chi^{(3)}$ is the effective component of the third-order nonlinear susceptibility tensor of the gas, and $\cos\phi$ is the relative phase between ω pulse and 2ω pulse. The relationship in Eq. (9) was experimentally demonstrated from an energy dependence measurement by Xie et al. in 2006 [19]. The THz amplitude is linearly increased with the intensity of ω pulse and is proportional to the square root of the intensity of 2ω pulse. Even though the four-wave-mixing model successfully offers an intuitive and straightforward description, it fails to explain some observations in experiments. For example, the occurrence of a clear threshold cannot be predicted by the model. Instead, the threshold should be associated with the photoionization process happened in the air. Additionally, the four-wave-mixing model is not indicative of the enhancement of THz radiation that caused by an applied asymmetric laser field.

In 2007, Kim et al. proposed a transient photocurrent model [20] that could solve the problems mentioned above. In this model, a net photocurrent produced by asymmetric optical fields through the photoionization radiates THz waves. Compared with THz wave generation from gas plasmas induced by one-color laser pulses, the asymmetric electron motion introduced by the two-color laser fields leads to a net dipole moment and hence, much stronger THz emission.

In 2009, Karpowicz and Zhang developed a full quantum model [23] to depict a complete physical picture of the generation process by numerically solving the time-dependent Schrödinger equation. The model accurately describes the formation and acceleration of the relevant wave packets.

Compared with other THz wave generation techniques, the two-color excitation scheme in gases provides the THz radiation with intense electrical fields (> 8 MV/cm) as well as broad spectral information (> 100 THz) [84–86].

In addition, the two-color laser pulses enable the coherent control of THz waves [87]. A femtosecond ω pulse generates a 2ω pulse while passing through a β -BBO crystal. The perpendicular polarized ω and 2ω pulses pass through an α -BBO with its slow axis aligned with the polarization of the ω beam and the fast axis aligned with the polarization of the 2ω beam. Thus, the 2ω pulse leads the ω pulse after passing through the β -BBO crystal [87]. A fused silica wedge pair is used to finely control the phase delay between the ω and 2ω pulses. Finally, a tunable dual-band wave plate is used to control the polarization of the ω beam and the 2ω beam.

Modulation of THz waves generated from air plasmas has been achieved by changing the relative phase between

ω and 2ω pulses via the phase compensator. The dependence of THz yield upon the relative phase in the case of gas plasmas was also investigated in Refs. [20–23,87,88]. Moreover, the two-color excitation scheme was applied to thin metal films to achieve coherent control [89].

It is worth underlining that Dey et al. also reported THz wave generation from liquids by focusing femtosecond laser pulses into a cuvette filled with target liquids [90]. Their observations also indicate that the laser-induced plasma formation in liquid materials plays a critical role in the THz wave generation process. The electrons ionized from water molecules are regarded as quasi-free electrons [74], and therefore the THz wave generation process in water resembles the process in air. Thus, the two-color excitation scheme should also work in liquid water. Stronger THz waves and corresponding modulation are expected by using the asymmetric excitation scheme in water as well. Manipulation of strong THz emission would have widespread applications in different research fields, such as THz nonlinear optics [91,92] and electron acceleration [93,94]. In the following sections, the THz wave generation from a thin water film under two-color laser excitation will be discussed.

3.2 Experimental setup of the two-color excitation scheme

The schematic diagram of the experimental setup is shown in Fig. 22. A femtosecond amplified Ti: sapphire laser with a central wavelength of 800 nm and a repetition rate of 1 kHz was used. Unless otherwise stated, the laser pulse duration used in this experiment was 58 fs. A β -BBO crystal was used for the generation of 2ω pulses through frequency-doubling, and an in-line phase compensator was applied to accurately control the relative phase between ω and 2ω pulses by changing the mechanical insertion of one of the fused silica wedges [87]. A phase compensator was

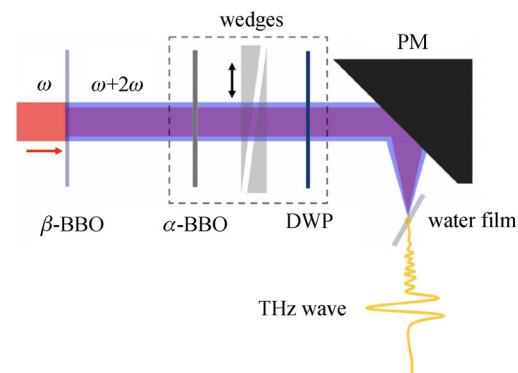


Fig. 22 Schematic diagram of the experimental setup. A phase compensator composed of an α -BBO crystal, a pair of wedges, and a dual-wavelength wave plate (DWP) is applied to control the relative phase between ω and 2ω pulses. PM, parabolic mirror with an effective focal length of 1-inch

composed of an α -BBO crystal, a pair of wedges, and a dual-wavelength wave plate (DWP). The energy of 2ω pulses was about 10% of the entire excitation laser energy. Both ω and 2ω pulses were vertically polarized after they pass through the phase compensator. Subsequently, ω and 2ω laser pulses were co-focused into a 120 μm thick water film by a 1-inch effective focal length parabolic mirror to generate THz waves. The focal point of the laser beam was set to be close to the center of the water film. A liquid jet was employed to obtain the water film. A high-resistivity silicon wafer was used as a filter to block the residual laser beams while allowing the THz waves to pass through. The THz electric field was detected by a 3 mm thick $\langle 110 \rangle$ -cut ZnTe crystal through EOS [52]. Also, the corresponding THz energy was measured by a commercially available Golay cell with a combination of different filters that eventually blocked all the high-frequency components. The angle of incidence on the water film was optimized to be 61° .

3.3 Comparison between terahertz radiation from one-color and two-color excitation scheme

By using the above experimental setup, THz emission from liquid water under the two-color excitation scheme is achieved. Remarkably, the THz electric field generated from the two-color excitation scheme is about 10-times stronger than that from the one-color excitation scheme at

the laser pulse duration of 58 fs, as shown in Fig. 23(a) [95]. The one-order of magnitude increased THz electric field is indicative of the two-orders of magnitude enhanced THz energy. The corresponding spectra are shown in Fig. 23(b). It is noteworthy that the enhancement of the THz electric field with the asymmetric excitation scheme in water may not be as high as that in air. This could arise from the fact that a short laser pulse duration works well for the case in air, but a longer pulse duration is favored in the ionization process in liquid water, where cascade ionization dominates [48,53,74].

Comparatively, experimental results in the case of a longer laser pulse duration (300 fs), which is obtained by chirping the original 58 fs pulse, are shown in Figs. 23(c) and 23(d). The scales of the vertical axis in Figs. 23(a) and 23(c) are the same. Compared to the one-color case, the two-color excitation scheme provides 11% enhanced THz electric field when the pulse duration is 300 fs. Such a reduced enhancement rate may be caused by multiple effects. For example, the ω and 2ω pulses may have uneven chirps, which reduces the asymmetry of the ionized electron motion and finally decreases the overall generation efficiency of THz waves. The lower enhancement with a longer pulse duration may also result from the significant drop in second-harmonic generation efficiency as the pulse duration increases. In the experiment, the energy of 2ω pulse decreases by more than 60% when the pulse duration increases from 58 to 300 fs.

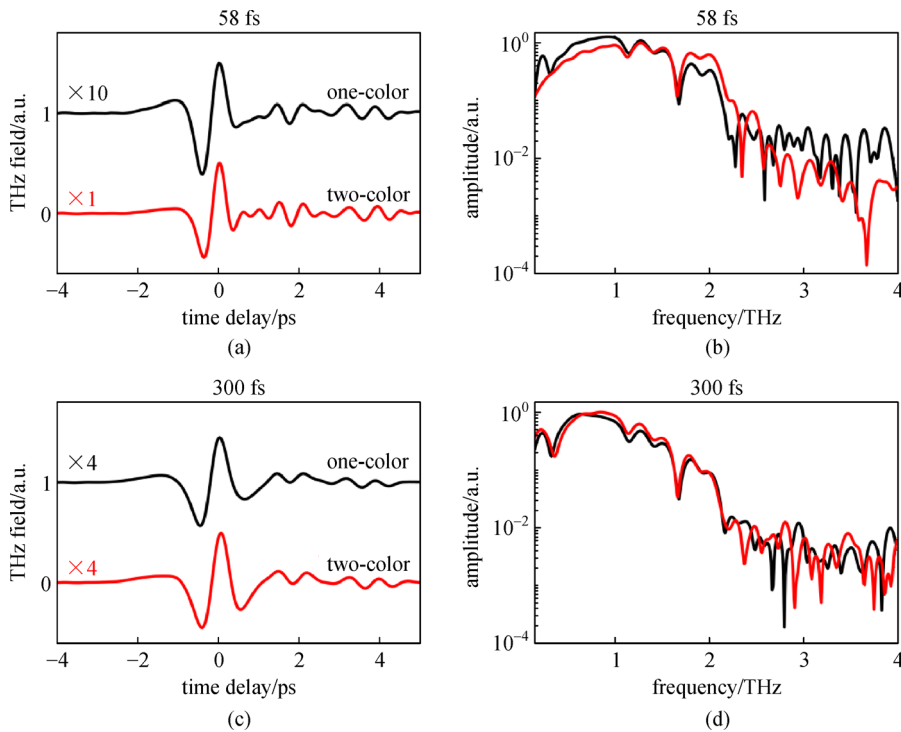


Fig. 23 Comparison of THz waves generated from a 120 μm thick water film with one-color and two-color excitation schemes [95]. (a) and (b) Comparison in the case of a short optical pulse duration (58 fs) in the time domain and frequency domain, respectively. (c) and (d) Comparison in the case of a long optical pulse duration (300 fs) in the time domain and frequency domain, respectively. Unified normalization ratios are labeled

3.4 Modulation of THz fields

Phenomenologically, the transient photocurrent model can be used to explain the generation process in water and would predict the modulation of THz fields generated from a water film as well, which is experimentally confirmed, as shown in Fig. 24 [95]. Specifically, Fig. 24(a) shows that the polarity of the THz electric field is completely flipped over by changing the relative phase φ by π . The inset of Fig. 24(a) plots the THz field as a function of optical phase delay between ω and 2ω pulses, which indicates that the polarity of the THz electric field is gradually changed with the optical phase delay.

Moreover, an overall phase scan for THz wave emission from the water film is obtained by gradually adjusting the phase between ω and 2ω pulses at an attosecond-level accuracy while monitoring the THz energy with a Golay cell, as shown in Fig. 24(b). The noise floor is also shown in Fig. 24(b). The modulated portion shows the phase modulation while the unmodulated portion remains blank at the bottom of the figure. By comparing the energy levels in the figure, the modulated and unmodulated components are estimated to be 70% and 30%, respectively. It needs to be mentioned that similar modulation can be achieved with

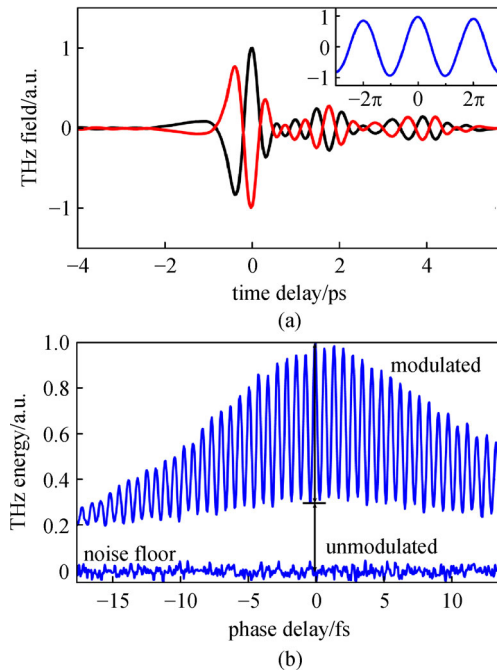


Fig. 24 Modulation of THz wave generation from a water film [95]. (a) Comparison of THz waveforms obtained when the relative phase between ω and 2ω pulses is changed by π through the change of the insertion of one of the wedges in the phase compensator. Inset, THz electric field as a function of the phase delay between ω and 2ω pulses. (b) An overall phase scan for THz wave radiation from the water film obtained by gradually changing the phase between ω and 2ω pulses while monitoring the THz energy by using a Golay cell. The range of the phase delay is limited by the full length of the wedge

a longer optical pulse duration (300 fs) as well.

The modulated and unmodulated THz waves are related to different generation processes in the plasma. For the further study, the corresponding THz energy varies with the excitation laser pulse energy was measured. Figure 25 [95] plots the THz energy as a function of the total excitation pulse (ω and 2ω) energy. The unmodulated THz energy (red circles) shows a linear dependence on the laser pulse energy. For the modulated THz energy (blue dots), the modulation does not appear until the excitation pulse energy is beyond 200 μJ . Subsequently, the measurement matches a quadratic fitting above the threshold. In addition, the energy dependence measured from EOS (blue squares) is coincident with the modulated result from the Golay cell.

Similar to the case in air, the modulated THz energy mainly comes from electron acceleration [20–23] in the transient photocurrent model, while in the full quantum model, the modulated THz radiation may also result from the buildup of bremsstrahlung from electron-atom collisions [23]. In contrast, the unmodulated THz energy may arise from multiple physical processes. For instance, a spatial net charge distribution created by the ponderomotive force radiates THz waves [15]. Since no threshold is observed for the unmodulated portion, the THz wave emission can be attributed to part of the broadband radiation from the combination of thermal bremsstrahlung from electrons and electron-ion recombination [49]. Moreover, the energy dependence in Fig. 25 indicates that the ratio of the modulated THz energy to unmodulated THz energy increases with the laser pulse energy. The unmodulated component is stronger with weak excitation pulses while the modulated component will dominate if intense laser pulses are used.

In consideration of the fact that the liquid source can quickly replenish itself due to its fluidity, the THz wave emission can be dramatically scaled up by increasing the

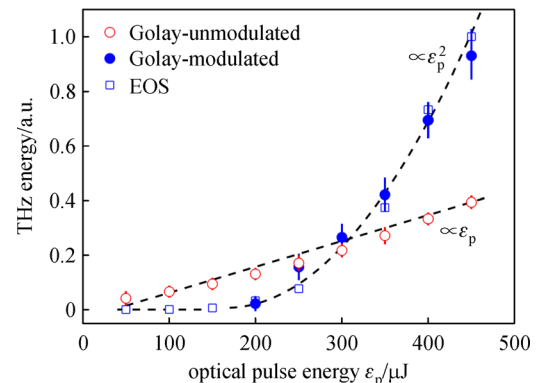


Fig. 25 Normalized THz energy from liquid water as a function of the total excitation optical pulse (ω and 2ω) energy [95]. Blue squares, THz energy calculated from the temporal integral of the THz waveform measured by EOS. Blue dots, modulated THz energy measured by the Golay cell. Red circles, unmodulated THz energy measured by the Golay cell. The maximum pulse energy is limited by the available laser pulse energy in the experiment

excitation laser energy, which reveals liquid water's potentiality to emit intense THz waves. Although no saturation occurs in Fig. 25 when the laser pulse energy is up to 450 μJ , it is worth mentioning that the saturation should be observed when the excitation energy is sufficiently high. The measured THz electric field strength is estimated as 1.1 kV/cm when the excitation laser pulse energy is 450 μJ . Realistically, the measured value is much weaker than the generated THz radiation due to the absorption of the water film itself and total internal reflection on the water-air boundary, etc.

3.5 Discussion about contributions from water and air

When the optical beam is focused into the water film, it will also possibly create air plasmas located close to the air-water interface and water-air interface. Thus, discussions are necessary to address the contributions from those air plasmas. Actually, the experiment in Section 2.3 has already been carried out to ensure that THz waves generated with this focusing geometry are primarily from the plasmas located inside the water film. In this experiment of two-color excitation, the focusing geometry is the same as that used in Section 2.3. The maximum excitation laser pulse energy 450 μJ is similar to that (400 μJ) used in Section 2.3. Moreover, the larger angle of incidence onto the water film increases the laser path length within the water film, which also helps to hold the majority of the plasmas inside the water film.

To further compare the THz wave emission from the water film (at the focus) and that from the air plasma (at the interface) in the experiment, the ratios of the corresponding THz electric field strength $E_a(z_i)/E_w(z_0)$ and THz power $P_a(z_i)/P_w(z_0)$ can be estimated. The subscript w represents water and a represents air. z_0 and z_i are the locations at the focus and the interface, respectively. It is assumed that no water is present when we estimate the values of E_a and P_a . The influence of the water film will be discussed later. Both the laser beam and the generated THz beam are assumed to have a Gaussian profile for this approximation.

Under the experimental condition, the laser intensity in the air at the focus is assumed to be $I(z_0) = 1 \times 10^{15} \text{ W/cm}^2$ [96,97]. The laser intensity $I(z_i)$ at the interface is calculated through $I(z_i) = I(z_0)[w(z_0)/w(z_i)]^2$, where $w(z_0)$ and $w(z_i)$ are the radii of the laser beam at the focus and the interface, respectively. Thus, the ratio of generated THz electric field strength from the air at the focus to that at the interface $E_a(z_i)/E_a(z_0)$ is calculated by the transient photocurrent model [20–22]. By experimentally measuring $E_a(z_0)$ and $E_w(z_0)$, the ratio $E_a(z_i)/E_w(z_0) = E_a(z_i)/E_a(z_0) \times E_a(z_0)/E_w(z_0) = 0.05\%$ is obtained. Then, the ratio of the THz intensity $I_a(z_i)/I_w(z_0)$ is calculated from $E_a(z_i)/E_w(z_0)$. Finally, the ratio of the THz power $P_a(z_i)/P_w(z_0) = 0.02\%$ can be obtained by integrating the corresponding THz intensity over its cross-section.

Consequently, the THz wave radiation from the air at the

interface is negligible, in comparison to the contribution from the water film. In fact, the measurable THz field from the air plasmas at the interfaces should be even smaller. Specifically, the water film will either absorb 83% of the THz energy from the plasma located close to the first interface (air-water) or decrease the laser intensity by affecting the focusing geometry for the plasma near the second interface (water-air). Based on the above discussion, THz waves generated in the experiment are mainly attributed to the plasma within the water film rather than the air plasma.

4 Terahertz wave generation from a water line

4.1 Issues of using water films

It was mentioned that a wire-guided free-flowing thin water film was developed to emit THz waves under the excitation of laser pulses. The observation shows that the film will be broken if high-energy laser pulses are focused onto it, therefore, the generation of intense THz radiation is restrained. To overcome this issue, a nozzle jet was used to produce a forced-flowing water film to bear intense laser pulses. Such an arrangement significantly increases the THz energy under intense optical excitation. However, a common problem occurred with the geometry of a film is that the majority of generated THz waves cannot be coupled out from the water film. Specifically, the THz signals are strongly absorbed by the millimeter-width water in the side-way directions. Aside from the absorption of water, the total internal reflection at the flat water-air interface will tremendously reduce the THz signals (see Fig. 12). Furthermore, due to the limitation in the fixed dimension of nozzle jets, water films with various thicknesses in a large range are not easily attainable, which impedes the systematical investigation on the optimal conditions for THz wave generation from liquid water. To ameliorate these drawbacks associated with using water films, water lines are introduced as the THz source. Currently, the THz field strength from a water line under single color-excitation was reported to be about 0.2 MV/cm with an efficiency of 0.06% [54]. These values are not great, compared with THz field strength, energy, and efficiency generated from other types of sources [14].

4.2 Water lines

Figure 26 shows a series of syringe needles (BSTEAN™) using to produce water lines. Inner diameters of the available syringe needles range from 0.06 to 1.65 mm. The gauge number/inner diameter of a syringe needle is represented by its color. A Masterflex L/S Digital Pump from Cole-Parmer® was utilized to drive the water to form the water line flowing along the y-direction.



color	gauge #	diameter/nm
oliver green	14	1.65
amber	15	1.40
green	18	0.84
pink	20	0.60
purple	21	0.51
blue	22	0.41
orange	23	0.33
red	25	0.26
white	27	0.21
light purple	30	0.16
yellow	32	0.09
lime green	34	0.06

Fig. 26 Photograph of syringe needles. The color of a syringe needle indicates its gauge number and inner diameter

Figure 27 is a photo of the water line produced by a syringe needle of 260 μm inner diameter. It is experimentally confirmed that the diameter of the top part of the water line is identical to the inner diameter of the syringe needle.

A femtosecond amplified Ti: sapphire laser with a central wavelength of 800 nm and a repetition rate of 1 kHz was used for the excitation. The flow velocity of the water line was controlled to be 7 m/s. In this case, each laser pulse interacted with a fresh water spot. The horizontally polarized laser beam with 0.4 mJ pulse energy propagating along the z -direction was focused into the water line by a 2-inch effective focal length lens (F/4) to generate THz waves. A high-resistivity silicon wafer acted as a filter to block the residual laser beam while allowing the THz beam passing through. The THz electric field was measured by a 2 mm thick $\langle 110 \rangle$ -cut ZnTe crystal placed in the direction of laser propagation through EOS [52].

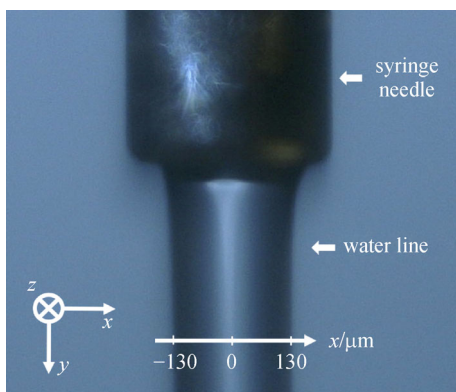


Fig. 27 Photograph of the water line produced by a syringe needle with 260 μm inner diameter [98]. The diameter of the water line is 260 μm as well. The flow velocity is about 7 m/s along the y -direction. The laser beam propagates in the z -direction. The water line can be moved along the x -direction by a translation stage

4.3 THz radiation from the water line

Figure 28(a) [98] shows the peak values of THz fields when the 260 μm diameter water line is scanned along the x -direction across the laser focal point. A weak THz signal is detected at $x = 0 \mu\text{m}$, which is represented as the black dot in the middle. This coincides with the case of a water film with a normally incident laser beam. By contrast, the THz signal becomes significant when the water line is shifted away from the zero position in the x -direction. The THz field is maximized at $x = \pm 90 \mu\text{m}$, which is caused by the ponderomotive force-induced current with the symmetry broken around the interface [54]. The value of the THz peak field changes in sign from negative (red dots) to positive (blue dots) when the x position varies from negative to positive. If two points are symmetric about 0, their absolute values of THz peak field are identical.

The waveforms of the THz signals at $x = \pm 90 \mu\text{m}$ are shown in Fig. 28(b). Clearly, the THz waveforms flip over when their x positions are mirrored with respect to the zero position. The results in Figs. 28(a) and 28(b) can also be understood from the dipole radiation model proposed earlier: mirrored x position leads to an opposite projected direction of the dipole in water, resulting in an inverted THz waveform. For $x = 0 \mu\text{m}$, the dipole in water is oriented along the direction of laser propagation contributing to weak THz radiation in the z -direction. Thus, a tilted dipole realized by a shift of the water line in the x -direction is essential to obtain the strongest THz signal in the direction of laser propagation. Note that unlike the case of a water film, THz signals generated from a water line can also be coupled out and detected in the x -direction. This will increase the overall coupling of the THz radiation.

To make a reasonable comparison between the THz waves generated from a water line and a water film, a 210 μm diameter water line and a 120 μm thick water film were used to assure that their optical effective path lengths

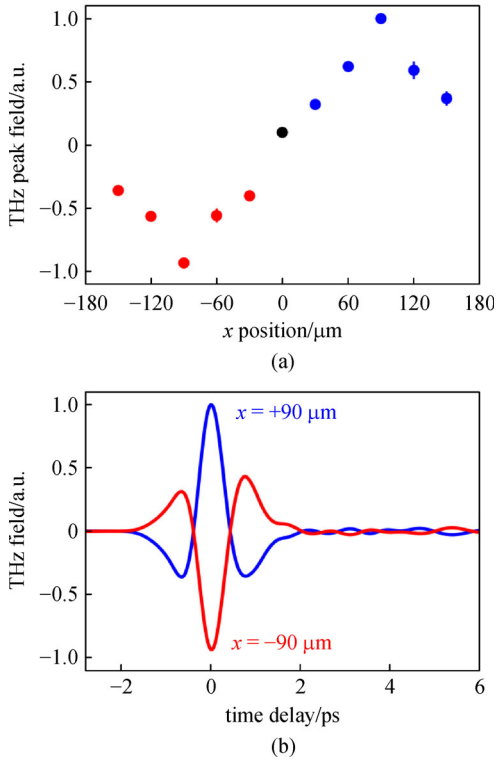


Fig. 28 (a) THz peak fields with different x positions when the $260\ \mu\text{m}$ diameter water line is crossing the laser focal point along the x -direction. (b) THz waveforms of $x = \pm 90\ \mu\text{m}$ in (a) [98]

(EPLs) in water were similar. The incident angle on the water film is 60° , which leads to the $151\ \mu\text{m}$ EPL in the film. The shift of the water line in the x -direction causes the EPL to be $158\ \mu\text{m}$. Figure 29 plots the THz waveforms generated from the two cases. 2.8-times enhanced THz electric field (peak-valley) is obtained by using the water line to substitute the water film. Compared with the flat water-air interface of a film, the curved interface of a water line helps to reduce the total internal reflection of the THz waves, and therefore, more THz radiation is coupled out and detected.

4.4 Preference for sub-picosecond laser pulses

It was shown that optically induced THz wave generation from air plasma generally requires a short temporal laser pulse. In contrast, THz radiation from water prefers a longer pulse, wherein the mechanism remains unclear.

Benefited from the availability of a series of syringe needles with various sizes, water lines with diameters varied from tens of microns to a few millimeters are realized, which offer the opportunity for a thorough investigation into the influence of optical pulse duration on THz wave generation from liquid water.

To explore the dependence of THz radiation on the optical pulse duration, laser pulses were stretched in time to achieve various pulse durations τ_p . Corresponding THz

energy from a $210\ \mu\text{m}$ diameter water line was recorded and shown as the black dot in Fig. 30 [98]. Unlike the case of air, the optimization for THz radiation from liquid water prefers a sub-picosecond laser pulse (345 fs). In this article, “sub-picosecond” is defined as 200–800 fs.

The result of the optimal pulse duration can be understood from the interaction between the laser field and the water. Electrons are produced by intense laser pulses through MPI/TI and cascade ionization at the focus. It is worth underlining that each cascade process needs an ionization time $K\tau$ [74] to perform. Thus, one seed electron cannot produce more than $2^{\tau_p/(K\tau)}$ electrons through the cascade process, regardless of the laser intensity. Compared with the increase in the number of electrons due to MPI/TI, the exponential boost caused by cascade ionization makes it the dominating ionization process in water when τ_p is above 40 fs [74]. Therefore, a longer pulse duration that allows more cascades taking place benefits plasma formation through the exponential increase from cascade ionization. Even though the majority of electrons are provided by cascade ionization, MPI/TI is still quite important because it provides most of the electrons to initiate the cascade process, especially in pure water. Since MPI/TI highly depends on laser intensity and laser intensity is inversely proportional to τ_p when the laser pulse energy ε_p is fixed, generated electron density will start to decrease if τ_p raises too much. Considering the fact that higher electron density contributes to more THz radiation, the trade-off between the two effects can lead to the preference for sub-picosecond pulses.

Simulations that based on Eqs. (2) and (3) are carried out to verify the theoretical analysis. The laser wavelength and pulse energy are set to match the values in the experiment (see Section 4.2). The laser intensity at the focus is calculated to be at the level of $10^{15}\ \text{W}/\text{cm}^2$. In such a case, the Keldysh parameter $\gamma = 0.2$ implies that TI dominates over MPI. In the experiment, a strong external focusing is

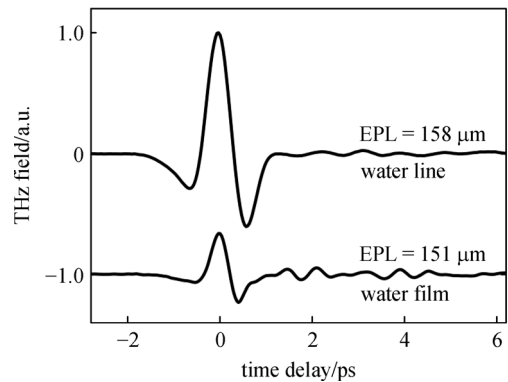


Fig. 29 Comparison of THz fields generated from a $210\ \mu\text{m}$ water line and a $120\ \mu\text{m}$ water film. EPL, effective path length. A shift of the $210\ \mu\text{m}$ water line in the x -direction makes the EPL to be $158\ \mu\text{m}$. Oblique incidence on the $120\ \mu\text{m}$ water film leads to a $151\ \mu\text{m}$ EPL

used, where the SF and the geometrical focusing become indistinguishable [99]. Thus, the term of SF is not included in the simulation. The impact of GVD is assumed to be insignificant because the plasma length of our interest is short ($\sim 200 \mu\text{m}$). A commonly used value of electron collision time $\tau = 1 \text{ fs}$ is applied [74]. Water is treated as an amorphous semiconductor with a bandgap of $E_g = 6.5 \text{ eV}$. Since femtosecond and sub-picosecond laser pulses are used in the experiment, contribution from diffusion is justifiably neglected [74,77]. The TI ionization rate w and the cascade ionization rate η_{cas} are calculated by Eqs. (6) and (7) respectively. The recombination rate η_{rec} is taken to be $2 \times 10^9 \text{ cm}^3/\text{s}$ [74,100]. The molecular density of water is $3.34 \times 10^{22} \text{ cm}^3$ [48]. The initial electron density is chosen to be $\rho_0 = 10^{10} \text{ cm}^3$, which will hardly impact on the evolution of electron density even if ρ_0 is changed over several orders of magnitude [77,101]. By numerically solving [77] the coupled Eqs. (2) and (3) with different values of pulse duration, the evolution of electron density $\rho(z,t)$ that corresponds to different τ_p is obtained. Consequently, the peak electron density versus τ_p is achieved and plotted as the red curve in Fig. 30. As expected, a sub-picosecond pulse is a requisite for the highest peak electron density.

For further verification, the diameter of the water line d is chosen as a variable to see how the optimal pulse duration changes with the water line diameter in the experiment and simulation. Experimentally, seven individual syringe needles with different inner diameters were used to produce water lines with diameters varying from tens of microns to half a millimeter. The optimal pulse duration for the THz energy from each water line was recorded and shown as the red dot in Fig. 31 [98]. The optimal pulse duration gradually changes from 257 to 513 fs when d increases from 90 to 510 μm . In the simulation, the evolution of electron density that corresponds to different τ_p is achieved. Then the peak electron density is

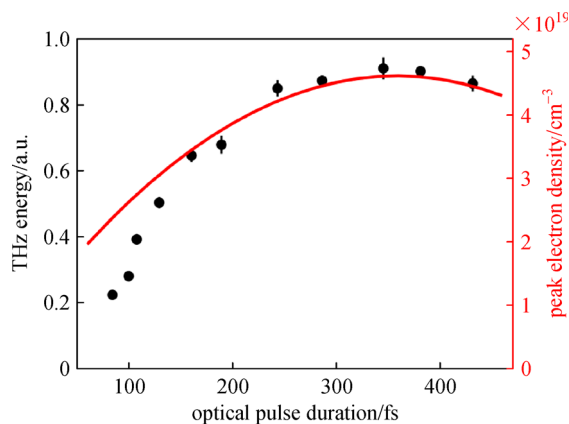


Fig. 30 Effect of optical pulse duration on THz energy and peak electron density for a 210 μm water line [98]. The black dots are the experimental data for THz energy. The red curve is the simulation data for peak electron density

integrated over z within the whole range of the water line that is determined by the diameter d . Thus, the optimal pulse duration for the highest electron density that corresponds to the different diameter of the water line is obtained (see the blue squares) in Fig. 31. To make the result clear to see, only a few points in a similar range of the experiment are shown. The coincidence of the experimental result and the simulation supports the model and the explanation.

The corresponding THz energy from each water line is plotted in Fig. 32. The maximum THz energy is obtained with a 210 μm diameter water line, which results from the trade-off between laser-water interaction length and absorption of water for THz waves. Specifically, a very thin water line does not have sufficient length for the interaction between laser pulses and water molecules while a very thick water line suffers from serious absorption. Neither case does offer strong THz radiation. Note that the THz energy slightly decreases rather than significantly drops when the diameter of the water line increases from 330 to 510 μm . The reason is that during the optimization process for the maximal THz signal, the water line was

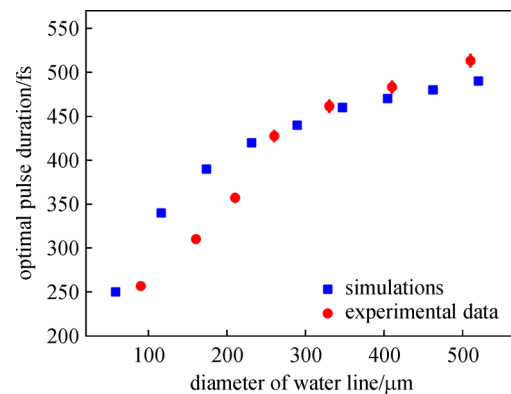


Fig. 31 Optimal optical pulse duration versus the diameter of the water line [98]. The blue squares are simulations of optimal pulse duration aiming for the highest electron density. The red dots are the experimental data of optimal pulse duration obtained with the strongest THz energy

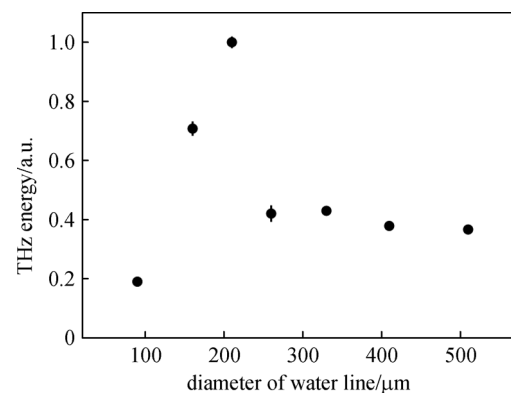


Fig. 32 THz energy versus the diameter of the water line

moved toward the incoming laser beam along the z -direction to compensate for the absorption of water. Consequently, the laser focal point was close to the second interface (water-air interface) instead of being located at the center of the water line. No increment of the THz energy is observed when the water line's diameter raises from 330 to 510 μm , which reveals that further extension of the interaction length no longer helps.

It needs to be mentioned that the demonstration of the preference for sub-picosecond optical pulses can also be used to explain the low enhancement of the THz radiation under the two-color excitation. Sub-picosecond pulses are indispensable to achieve high electron density in water. Nevertheless, a short pulse works much better for the second-harmonic generation from the fundamental beam. The discrepant demand regarding the pulse duration significantly limits the generation of THz waves under the two-color excitation. Therefore, an intense THz radiation could be expected if the requirements for pulse duration are satisfied under the two-color excitation. One possible solution is separately controlling the phase and polarization [102] of the fundamental beam and the second-harmonic beam by using a dichroic mirror. Another dichroic mirror can be applied to combine the second-harmonic beam and the stretched fundamental beam. Such an arrangement assures that the plasma would be generated by a time-stretched pulse and the second harmonic component remains intense.

5 Terahertz wave generation from α -Pinene

5.1 α -Pinene

To make sure that there are enough THz waves can be coupled out from the generation site for the detection, a thin water film or water line has been utilized as the THz emitter in the previous sections. Another approach to avoid suffering from the strong absorption is to use a liquid with weaker absorption in the THz frequency regime as the source.

α -Pinene is a popular non-polar liquid, which can be found in the oils of the pine. It is an organic compound of the terpene class. Nontoxic and colorless α -Pinene makes it a good candidate for the THz emitter. Before using α -Pinene to generate THz waves, it is essential to ensure its weak absorption property within the frequency region of interest.

A standard THz-TDS system was used for measurement [103]. The red curve in Fig. 33 shows the THz waveform with a 1 mm thick α -Pinene sample. As a reference, the black curve is the measured THz waveform without the sample. The different field amplitude results from the absorption of THz waves, the time shift is caused by the different refractive indices of the air and the sample. The information in the frequency domain can be obtained

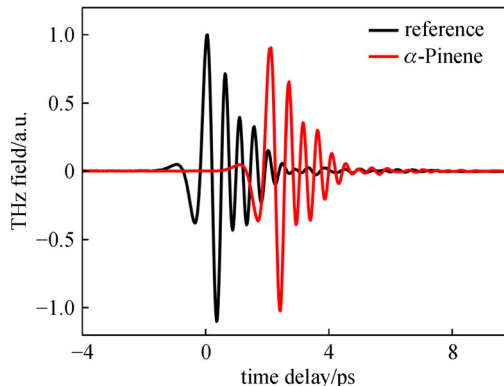


Fig. 33 Waveform measurement of α -Pinene as the sample by using a standard THz-TDS system. The black curve is the reference waveform with no sample presented

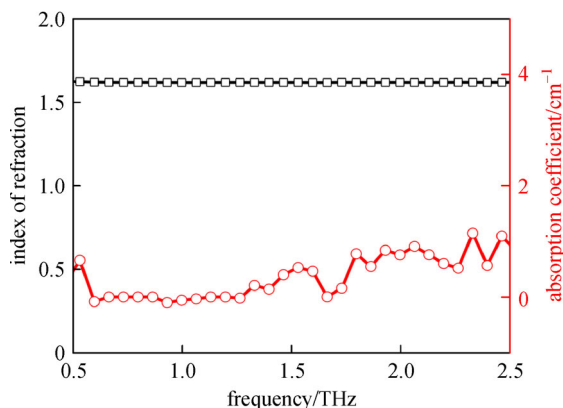


Fig. 34 Measured results of refractive index and field absorption coefficient of α -Pinene in the frequency region 0.5–2.5 THz [98]

through the Fourier transform, which is utilized to calculate the frequency-dependent index of refraction and field absorption coefficient of the sample. The result is shown in Fig. 34.

The black squares in Fig. 34 plot the index of refraction versus the frequency. α -Pinene has a refractive index of 1.62 from 0.5 to 2.5 THz with little dispersion. The red circles show that the field absorption coefficient of α -Pinene in such a frequency regime is less than 2 cm^{-1} . A few points showing negative values of absorption coefficient may result from system error when the absorption is very weak. Compared with the value of water, the absorption coefficient of α -Pinene is impressively small.

5.2 Comparison between terahertz radiation from α -Pinene and water

Since the absorption of α -Pinene is much weaker than that of water, a stronger THz signal is expected to be obtained from α -Pinene. It is worth underlining that α -Pinene is too

viscous to be used to form a stable free-flowing film for the generation of THz waves. Thus, a syringe needle was applied to form a forced-flowing α -Pinene line. The experimental setup is the same as the one described in Section 4.2. The diameter of the liquid line is 210 μm . Laser pulse energy is 0.4 mJ with the optimal pulse duration around 345 fs. THz radiation generated from an α -Pinene line and a water line were recorded for comparison. Figure 35(a) shows the measured time domain waveforms. Their Fourier transform offers the information in the frequency domain (see Fig. 35(b)) [98].

Figure 35 shows that α -Pinene emits a stronger THz field, which is about 1.8-times stronger than that from water in the identical experimental condition (liquid lines diameter, laser pulse energy, laser pulse duration, etc.). The electric field strength of THz waves generated by the 210 μm diameter α -Pinene line is estimated to be 0.7 kV/cm through EOS [50]. In the frequency domain, α -Pinene offers more high-frequency (above 1 THz) components and provides a wider bandwidth.

The significant difference in absorption characteristics between water and α -Pinene is the main reason that causes their difference in Fig. 35. To see whether it is the only

contributor or not, the absorption from α -Pinene is removed from the experimental data (black curve) and the absorption from water is added [24]. This treatment of ignoring the change of absorption caused by the plasma formation is justified because only 0.2% of molecules are ionized in this case. The influence of their different refractive indices on the Fresnel coefficients of the interfaces is included. The result is plotted as the blue dash line in Fig. 35(b). The discrepancy between the blue dash line and the red curve reveals that there are other contributors involved.

Many other parameters (such as refractive index, ionization energy, ionization time, collision time, molecule mass, and molecular density) of liquids function in the ionization process, and thus may affect the THz radiation resulting in the observation in Fig. 35(b). Further investigation into plasma current [104,105] and plasma radiation [106] for THz waves is needed to fully understand the result in Fig. 35.

6 Conclusions

The work of using liquid water to generate THz radiation is reviewed. Some other important topics about THz wave generation from water should also be highlighted here. Ponomareva et al. and Tcypkin et al. investigated the efficiency of THz wave generation from water [107,108]. A preformed plasma was demonstrated as an alternative method to enhance the THz radiation from water [109–111]. As previously mentioned, the THz field strength generated from water was reported to be 0.2 MV/cm by Zhang et al. [54]. Huang et al. used water jets to generate both THz radiation and X-ray [111,112].

It should be noted that laser-induced plasma in water plays a significant role in the generation process even though the source is originally in the liquid form. This work not only paves the way for developing intense THz sources but also has contributed to enthralling insight into the study of laser-water interaction.

Broadband THz wave generation from a water film was shown. Mechanism of the generation process is attributed to laser-induced plasma formation in water associated with a ponderomotive force-induced dipole radiation model. Specifically, it is observed that THz radiation from liquid water prefers sub-picosecond laser pulses for the excitation, which can be fully explained by the process of laser-induced plasma formation in water. Furthermore, measurement of the THz radiation pattern matches well with the simulation predicted by the dipole radiation model.

THz emission from a water film under the two-color excitation scheme was also discussed. One-order of magnitude stronger THz electric field is obtained by using the asymmetric excitation scheme with short temporal laser pulses. The modulation of THz waves is achieved by adjusting the relative phase between ω and 2ω

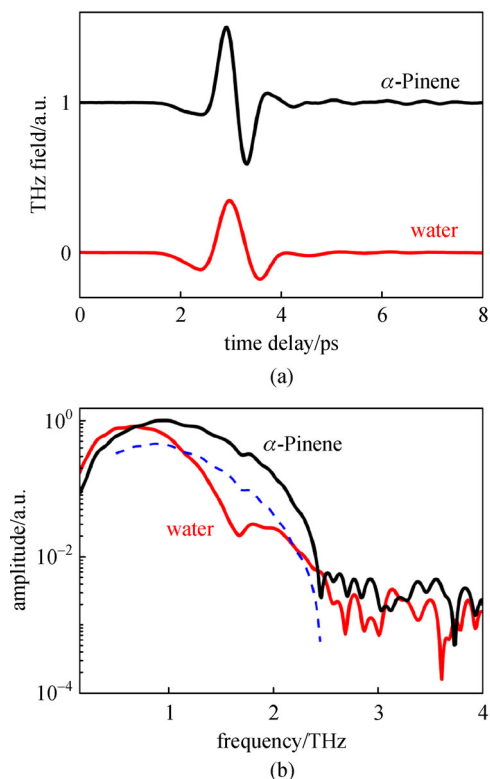


Fig. 35 Comparison of THz waves generated from α -Pinene and water in (a) time domain and (b) frequency domain [98]. The diameter of the liquid line is 210 μm . Laser pulse energy is 0.4 mJ. Optical pulse durations are individually optimized for α -Pinene and water. Both have a value around 345 fs. The dash line in (b) is calculated by removing the absorption of α -Pinene and adding the absorption of water to the black curve from 0.5 to 2.5 THz

pulses. The method also enables the observation of modulated and unmodulated THz waves with a Gouy cell. By increasing the excitation pulse energy, the unmodulated component is linearly raised while the modulated component is quadratically enhanced above the threshold, which indicates that the THz yield can be dramatically scaled up by increasing the excitation pulse energy.

To mitigate the total internal reflection at the water-air interface of water films, water lines produced by syringe needles were applied to achieve stronger THz signals. It is found that the optimal laser pulse duration highly depends upon the diameter of the water line, which also impacts on the THz radiation energy. The maximum THz signal is obtained with a 210 μm diameter water line.

As a supplement to the study of terahertz aqueous photonics, THz wave generation from α -Pinene was presented. α -Pinene generates a 1.8-times stronger THz electric field with a wider bandwidth than water does. The stronger THz radiation mainly results from the fact that α -Pinene almost does not absorb THz waves. It needs to be highlighted that THz wave generation from the water is stronger than that from the air with the one-color excitation scheme, which is coincident as the expectation from the higher molecule density of water. However, water is no longer the winner with the two-color excitation scheme. In water, cascade ionization favors a long pulse duration (sub-picosecond) to exponentially produce electrons. But the second-harmonic generation efficiency from the fundamental laser pulse significantly drops as the optical pulse duration increases. The discrepant demand regarding the pulse duration significantly limits the generation of THz waves under the two-color excitation. However, from the perspective of the development of intense liquid THz sources, the two-color excitation scheme may still be the way to go. Wise management of laser pulse duration is imperative. It should be noticed that only a few types of liquids have been tested so far. The best liquid source for THz radiation may still be out of the scope. Systematical tests of other liquids are necessary. Commercializing a compact liquid THz source is an interesting and promising topic as well. Moreover, developing a liquid THz sensor can be a challenging project to further the research of terahertz aqueous photonics.

Acknowledgements This research was sponsored by the Army Research Office under Grant No. W911NF-17-1-0428, Air Force Office of Scientific Research under Grant No. FA9550-18-1-0357, and National Science Foundation under Grant No. ECCS-1916068.

References

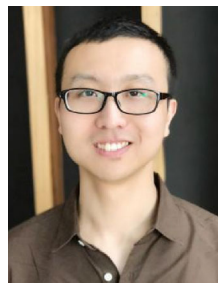
1. Wang T, Klarskov P, Jepsen P U. Ultrabroadband THz time-domain spectroscopy of a free-flowing water film. *IEEE Transactions on Terahertz Science and Technology*, 2014, 4(4): 425–431

2. Lee Y S. *Principles of Terahertz Science and Technology*. Vol. 170. New York: Springer US, 2009
3. Mittleman D M. Twenty years of terahertz imaging. *Optics Express*, 2018, 26(8): 9417–9431
4. Zhao J, E Y, Williams K, Zhang X C, Boyd R W. Spatial sampling of terahertz fields with sub-wavelength accuracy via probe-beam encoding. *Light, Science & Applications*, 2019, 8(1): 55
5. Look D C. Molecular beam epitaxial GaAs grown at low temperatures. *Thin Solid Films*, 1993, 231(1–2): 61–73
6. Beard M C, Turner G M, Schmuttenmaer C A. Subpicosecond carrier dynamics in low-temperature grown GaAs as measured by time-resolved terahertz spectroscopy. *Journal of Applied Physics*, 2001, 90(12): 5915–5923
7. Boyd R W. *Nonlinear Optics*. 2nd ed. New York: Academic Press, 2003
8. Hebling J, Almasi G, Kozma I, Kuhl J. Velocity matching by pulse front tilting for large area THz-pulse generation. *Optics Express*, 2002, 10(21): 1161–1166
9. Hebling J, Yeh K L, Hoffmann M C, Bartal B, Nelson K A. Generation of high-power terahertz pulses by tilted-pulse-front excitation and their application possibilities. *Journal of the Optical Society of America B, Optical Physics*, 2008, 25(7): B6–B19
10. Fülöp J A, Pálfalvi L, Klingebiel S, Almási G, Krausz F, Karsch S, Hebling J. Generation of sub-mJ terahertz pulses by optical rectification. *Optics Letters*, 2012, 37(4): 557–559
11. Zhang X C, Ma X, Jin Y, Lu T M, Boden E P, Phelps P D, Stewart K R, Yakymyshyn C P. Terahertz optical rectification from a nonlinear organic crystal. *Applied Physics Letters*, 1992, 61(26): 3080–3082
12. Hauri C P, Ruchert C, Vicario C, Ardana F. Strong-field single-cycle THz pulses generated in an organic crystal. *Applied Physics Letters*, 2011, 99(16): 161116
13. Shalaby M, Hauri C P. Demonstration of a low-frequency three-dimensional terahertz bullet with extreme brightness. *Nature Communications*, 2015, 6(1): 5976
14. Fülöp J A, Tzortzakos S, Kampfrath T. Laser-driven strong-field terahertz sources. *Advanced Optical Materials*, 2020, 8(3): 1900681
15. Hamster H, Sullivan A, Gordon S, White W, Falcone R W. Subpicosecond, electromagnetic pulses from intense laser-plasma interaction. *Physical Review Letters*, 1993, 71(17): 2725–2728
16. Hamster H, Sullivan A, Gordon S, Falcone R W. Short-pulse terahertz radiation from high-intensity-laser-produced plasmas. *Physical Review E: Statistical Physics, Plasmas, Fluids, and Related Interdisciplinary Topics*, 1994, 49(1): 671–677
17. Cook D J, Hochstrasser R M. Intense terahertz pulses by four-wave rectification in air. *Optics Letters*, 2000, 25(16): 1210–1212
18. Johnson K, Price-Gallagher M, Mamer O, Lesimple A, Fletcher C, Chen Y, Lu X, Yamaguchi M, Zhang X C. Water vapor: an extraordinary terahertz wave source under optical excitation. *Physics Letters A*, 2008, 372(38): 6037–6040
19. Xie X, Dai J, Zhang X C. Coherent control of THz wave generation in ambient air. *Physical Review Letters*, 2006, 96(7): 075005
20. Kim K Y, Glowacki J H, Taylor A J, Rodriguez G. Terahertz emission from ultrafast ionizing air in symmetry-broken laser fields. *Optics Express*, 2007, 15(8): 4577–4584

21. Kim K Y, Taylor A, Glowina J, Rodriguez G. Coherent control of terahertz supercontinuum generation in ultrafast laser–gas interactions. *Nature Photonics*, 2008, 2(10): 605–609
22. Kim K Y. Generation of coherent terahertz radiation in ultrafast laser-gas interactions. *Physics of Plasmas*, 2009, 16(5): 056706
23. Karpowicz N, Zhang X C. Coherent terahertz echo of tunnel ionization in gases. *Physical Review Letters*, 2009, 102(9): 093001
24. Ronne C, Thrane L, Åstrand P O, Wallqvist A, Mikkelsen K V, Keiding S R. Investigation of the temperature dependence of dielectric relaxation in liquid water by THz reflection spectroscopy and molecular dynamics simulation. *Journal of Chemical Physics*, 1997, 107(14): 5319–5331
25. Thrane L, Jacobsen R H, Uhd Jepsen P, Keiding S R. THz reflection spectroscopy of liquid water. *Chemical Physics Letters*, 1995, 240(4): 330–333
26. Kotz J C, Treichel P M, Townsend J. *Chemistry and Chemical Reactivity*. Raleigh, NC: Cengage Learning, 2012
27. Engels D, Schmid-Burgk J, Walmsley C. Water maser emission from OH/IR stars. *Astronomy & Astrophysics*, 1986, 167: 129–144
28. Neufeld D A, Melnick G J. Excitation of millimeter and submillimeter water masers. *Astrophysical Journal*, 1991, 368: 215–230
29. Neufeld D A, Maloney P R, Conger S. Water maser emission from X-ray-heated circumnuclear gas in active galaxies. *Astrophysical Journal*, 1994, 436: 127–130
30. Alfano R R, Shapiro S. Observation of self-phase modulation and small-scale filaments in crystals and glasses. *Physical Review Letters*, 1970, 24(11): 592–594
31. Jimbo T, Caplan V L, Li Q X, Wang Q Z, Ho P P, Alfano R R. Enhancement of ultrafast supercontinuum generation in water by the addition of Zn^{2+} and K^+ cations. *Optics Letters*, 1987, 12(7): 477–479
32. Kandidov V, Kosareva O, Golubtsov I, Liu W, Becker A, Akozbek N, Bowden C M, Chin S L. Self-transformation of a powerful femtosecond laser pulse into a white-light laser pulse in bulk optical media (or supercontinuum generation). *Applied Physics B, Lasers and Optics*, 2003, 77(2–3): 149–165
33. Liu W, Petit S, Becker A, Aközbek N, Bowden C M, Chin S L. Intensity clamping of a femtosecond laser pulse in condensed matter. *Optics Communications*, 2002, 202(1–3): 189–197
34. Dharmadhikari A, Rajgara F, Mathur D. Systematic study of highly efficient white light generation in transparent materials using intense femtosecond laser pulses. *Applied Physics B, Lasers and Optics*, 2005, 80(1): 61–66
35. Kaya N, Strohaber J, Kolomenskii A A, Kaya G, Schroeder H, Schuessler H A. White-light generation using spatially-structured beams of femtosecond radiation. *Optics Express*, 2012, 20(12): 13337–13346
36. Dharmadhikari J A, Steinmeyer G, Gopakumar G, Mathur D, Dharmadhikari A K. Femtosecond supercontinuum generation in water in the vicinity of absorption bands. *Optics Letters*, 2016, 41(15): 3475–3478
37. Attwood D, Sakdinawat A. *X-rays and Extreme Ultraviolet Radiation: Principles and Applications*. Cambridge: Cambridge University Press, 2017
38. McNaught S, Fan J, Parra E, Milchberg H M. A pump–probe investigation of laser-droplet plasma dynamics. *Applied Physics Letters*, 2001, 79(25): 4100–4102
39. Düsterer S, Schwoerer H, Ziegler W, Ziener C, Sauerbrey R. Optimization of EUV radiation yield from laser-produced plasma. *Applied Physics B, Lasers and Optics*, 2001, 73(7): 693–698
40. Kurz H G, Steingrube D S, Ristau D, Lein M, Morgner U, Kovačev M. High-order-harmonic generation from dense water microdroplets. *Physical Review A*, 2013, 87(6): 063811
41. Flettner A, Pfeifer T, Walter D, Winterfeldt C, Spielmann C, Gerber G. High-harmonic generation and plasma radiation from water microdroplets. *Applied Physics B, Lasers and Optics*, 2003, 77(8): 747–751
42. Donnelly T D, Rust M, Weiner I, Allen M, Smith R A, Steinke C A, Wilks S, Zweiback J, Cowan T E, Ditmire T. Hard X-ray and hot electron production from intense laser irradiation of wavelength-scale particles. *Journal of Physics B, Atomic, Molecular, and Optical Physics*, 2001, 34(10): L313–L320
43. Malmqvist L, Rymell L, Hertz H M. Droplet-target laser-plasma source for proximity X-ray lithography. *Applied Physics Letters*, 1996, 68(19): 2627–2629
44. Berglund M, Rymell L, Hertz H M. Ultraviolet prepulse for enhanced X-ray emission and brightness from droplet-target laser plasmas. *Applied Physics Letters*, 1996, 69(12): 1683–1685
45. Rymell L, Hertz H M. Droplet target for low-debris laser-plasma soft X-ray generation. *Optics Communications*, 1993, 103(1–2): 105–110
46. Nikogosyan D N, Oraevsky A A, Rupasov V I. Two-photon ionization and dissociation of liquid water by powerful laser UV radiation. *Chemical Physics*, 1983, 77(1): 131–143
47. Crowell R A, Bartels D M. Multiphoton ionization of liquid water with 3.0–5.0 eV photons. *Journal of Physical Chemistry*, 1996, 100(45): 17940–17949
48. Kennedy P K. A first-order model for computation of laser-induced breakdown thresholds in ocular and aqueous media. I. Theory. *IEEE Journal of Quantum Electronics*, 1995, 31(12): 2241–2249
49. Kennedy P K, Hammer D X, Rockwell B A. Laser-induced breakdown in aqueous media. *Progress in Quantum Electronics*, 1997, 21(3): 155–248
50. Hirori H, Doi A, Blanchard F, Tanaka K. Single-cycle terahertz pulses with amplitudes exceeding 1 MV/cm generated by optical rectification in LiNbO_3 . *Applied Physics Letters*, 2011, 98(9): 091106
51. Blanchard F, Razzari L, Bandulet H C, Sharma G, Morandotti R, Kieffer J C, Ozaki T, Reid M, Tiedje H F, Haugen H K, Hegmann F A. Generation of 1.5 μJ single-cycle terahertz pulses by optical rectification from a large aperture ZnTe crystal. *Optics Express*, 2007, 15(20): 13212–13220
52. Wu Q, Zhang X C. Free-space electro-optic sampling of terahertz beams. *Applied Physics Letters*, 1995, 67(24): 3523–3525
53. Jin Q, E Y, Williams K, Dai J, Zhang X C. Observation of broadband terahertz wave generation from liquid water. *Applied Physics Letters*, 2017, 111(7): 071103
54. Zhang L L, Wang W M, Wu T, Feng S J, Kang K, Zhang C L,

- Zhang Y, Li Y T, Sheng Z M, Zhang X C. Strong terahertz radiation from a liquid-water line. *Physical Review Applied*, 2019, 12(1): 014005
55. Wang W M, Gibbon P, Sheng Z M, Li Y T. Integrated simulation approach for laser-driven fast ignition. *Physical Review E: Statistical, Nonlinear, and Soft Matter Physics*, 2015, 91(1): 013101
 56. Buccheri F, Zhang X C. Terahertz emission from laser-induced microplasma in ambient air. *Optica*, 2015, 2(4): 366–369
 57. Zhang J Z, Lam J K, Wood C F, Chu B T, Chang R K. Explosive vaporization of a large transparent droplet irradiated by a high intensity laser. *Applied Optics*, 1987, 26(22): 4731–4737
 58. Schaffer C, Nishimura N, Glezer E, Kim A, Mazur E. Dynamics of femtosecond laser-induced breakdown in water from femtoseconds to microseconds. *Optics Express*, 2002, 10(3): 196–203
 59. Courvoisier F, Boutou V, Favre C, Hill S C, Wolf J P. Plasma formation dynamics within a water microdroplet on femtosecond time scales. *Optics Letters*, 2003, 28(3): 206–208
 60. Lindinger A, Hagen J, Socaciu L D, Bernhardt T M, Wöste L, Duft D, Leisner T. Time-resolved explosion dynamics of H₂O droplets induced by femtosecond laser pulses. *Applied Optics*, 2004, 43(27): 5263–5269
 61. Stan C A, Milathianaki D, Laksmono H, Sierra R G, McQueen T A, Messerschmidt M, Williams G J, Koglin J E, Lane T J, Hayes M J, Guillet S A H, Liang M, Aquila A L, Willmott P R, Robinson J S, Gumerlock K L, Botha S, Nass K, Schlichting I, Shoeman R L, Stone H A, Boutet S. Liquid explosions induced by X-ray laser pulses. *Nature Physics*, 2016, 12(10): 966–971
 62. E Y, Jin Q, Tcypkin A, Zhang X C. Terahertz wave generation from liquid water films via laser-induced breakdown. *Applied Physics Letters*, 2018, 113(18): 181103
 63. Bebb H B, Gold A. Multiphoton ionization of hydrogen and rare-gas atoms. *Physical Review*, 1966, 143(1): 1–24
 64. DeMichelis C. Laser induced gas breakdown: a bibliographical review. *IEEE Journal of Quantum Electronics*, 1969, 5(4): 188–202
 65. Shen Y R. *The Principles of Nonlinear Optics*. New York: Wiley, 1984
 66. Lambropoulos P. Mechanisms for multiple ionization of atoms by strong pulsed lasers. *Physical Review Letters*, 1985, 55(20): 2141–2144
 67. Perry M D, Landen O L, Szöke A, Campbell E M. Multiphoton ionization of the noble gases by an intense 1014-W/cm² dye laser. *Physical Review A: General Physics*, 1988, 37(3): 747–760
 68. Keldysh L. Ionization in the field of a strong electromagnetic wave. *Soviet Physics, JETP*, 1965, 20(5): 1307–1314
 69. Ammosov M V. Tunnel ionization of complex atoms and of atomic ions in an alternating electromagnetic field. *Soviet Physics, JETP*, 1987, 64: 1191
 70. Bass M, Barrett H. Avalanche breakdown and the probabilistic nature of laser-induced damage. *IEEE Journal of Quantum Electronics*, 1972, 8(3): 338–343
 71. Bloembergen N. Laser-induced electric breakdown in solids. *IEEE Journal of Quantum Electronics*, 1974, 10(3): 375–386
 72. Morgan C G. Laser-induced breakdown of gases. *Reports on Progress in Physics*, 1975, 38(5): 621–665
 73. Puliafito C, Steinert R. Short-pulsed Nd:YAG laser microsurgery of the eye: biophysical considerations. *IEEE Journal of Quantum Electronics*, 1984, 20(12): 1442–1448
 74. Noack J, Vogel A. Laser-induced plasma formation in water at nanosecond to femtosecond time scales: calculation of thresholds, absorption coefficients, and energy density. *IEEE Journal of Quantum Electronics*, 1999, 35(8): 1156–1167
 75. Williams F, Varma S, Hillenius S. Liquid water as a lone-pair amorphous semiconductor. *Journal of Chemical Physics*, 1976, 64(4): 1549–1554
 76. Sacchi C. Laser-induced electric breakdown in water. *Journal of the Optical Society of America B, Optical Physics*, 1991, 8(2): 337–345
 77. Feng Q, Moloney J V, Newell A C, Wright E M, Cook K, Kennedy P K, Hammer D X, Rockwell B A, Thompson C R. Theory and simulation on the threshold of water breakdown induced by focused ultrashort laser pulses. *IEEE Journal of Quantum Electronics*, 1997, 33(2): 127–137
 78. Raïzer Y P. Reviews of topical problems: breakdown and heating of gases under the influence of a laser beam. *Soviet Physics Uspekhi*, 1966, 8(5): 650–673
 79. Hatanaka K, Ida T, Ono H, Matsushima S, Fukumura H, Juodkazis S, Misawa H. Chirp effect in hard X-ray generation from liquid target when irradiated by femtosecond pulses. *Optics Express*, 2008, 16(17): 12650–12657
 80. Dai J, Liu J, Zhang X C. Terahertz wave air photonics: terahertz wave generation and detection with laser-induced gas plasma. *IEEE Journal of Selected Topics in Quantum Electronics*, 2011, 17(1): 183–190
 81. Kreß M, Löffler T, Thomson M D, Dörner R, Gimpel H, Zrost K, Ergler T, Moshhammer R, Morgner U, Ullrich J, Roskos H G. Determination of the carrier-envelope phase of few-cycle laser pulses with terahertz-emission spectroscopy. *Nature Physics*, 2006, 2(5): 327–331
 82. Gaal P, Kuehn W, Reimann K, Woerner M, Elsaesser T, Hey R. Internal motions of a quasiparticle governing its ultrafast nonlinear response. *Nature*, 2007, 450(7173): 1210–1213
 83. Roskos H, Thomson M, Kreß M, Löffler T. Broadband THz emission from gas plasmas induced by femtosecond optical pulses: from fundamentals to applications. *Laser & Photonics Reviews*, 2007, 1(4): 349–368
 84. Oh T, Yoo Y, You Y, Kim K Y. Generation of strong terahertz fields exceeding 8 MV/cm at 1 kHz and real-time beam profiling. *Applied Physics Letters*, 2014, 105(4): 041103
 85. Thomson M D, Blank V, Roskos H G. Terahertz white-light pulses from an air plasma photo-induced by incommensurate two-color optical fields. *Optics Express*, 2010, 18(22): 23173–23182
 86. Zhang X C, Shkurinov A, Zhang Y. Extreme terahertz science. *Nature Photonics*, 2017, 11(1): 16–18
 87. Dai J, Karpowicz N, Zhang X C. Coherent polarization control of terahertz waves generated from two-color laser-induced gas plasma. *Physical Review Letters*, 2009, 103(2): 023001
 88. Wen H, Lindenberg A M. Coherent terahertz polarization control through manipulation of electron trajectories. *Physical Review*

- Letters, 2009, 103(2): 023902
89. Dai J, Zhang X C. Terahertz wave generation from thin metal films excited by asymmetrical optical fields. *Optics Letters*, 2014, 39(4): 777–780
 90. Dey I, Jana K, Fedorov V Y, Koulouklidis A D, Mondal A, Shaikh M, Sarkar D, Lad A D, Tzortzakis S, Couairon A, Kumar G R. Highly efficient broadband terahertz generation from ultrashort laser filamentation in liquids. *Nature Communications*, 2017, 8(1): 1184
 91. Shen Y, Watanabe T, Arena D A, Kao C C, Murphy J B, Tsang T Y, Wang X J, Carr G L. Nonlinear cross-phase modulation with intense single-cycle terahertz pulses. *Physical Review Letters*, 2007, 99(4): 043901
 92. Turchinovich D, Hvam J M, Hoffmann M C. Self-phase modulation of a single-cycle terahertz pulse by nonlinear free-carrier response in a semiconductor. *Physical Review B*, 2012, 85(20): 201304
 93. Nanni E A, Huang W R, Hong K H, Ravi K, Fallahi A, Moriena G, Dwayne Miller R J, Kärtner F X. Terahertz-driven linear electron acceleration. *Nature Communications*, 2015, 6(1): 8486
 94. Zhang D, Fallahi A, Hemmer M, Wu X, Fakhari M, Hua Y, Cankaya H, Calendron A L, Zapata L E, Matlis N H, Kärtner F X. Segmented terahertz electron accelerator and manipulator (STEAM). *Nature Photonics*, 2018, 12(6): 336–342
 95. Jin Q, Dai J, E Y, Zhang X C. Terahertz wave emission from a liquid water film under the excitation of asymmetric optical fields. *Applied Physics Letters*, 2018, 113(26): 261101
 96. Kiran P P, Bagchi S, Krishnan S R, Arnold C L, Kumar G R, Couairon A. Focal dynamics of multiple filaments: microscopic imaging and reconstruction. *Physical Review A*, 2010, 82(1): 013805
 97. Liu X L, Lu X, Liu X, Xi T T, Liu F, Ma J L, Zhang J. Tightly focused femtosecond laser pulse in air: from filamentation to breakdown. *Optics Express*, 2010, 18(25): 26007–26017
 98. Jin Q, E Y, Gao S, Zhang X C. Preference of subpicosecond laser pulses for terahertz wave generation from liquids. *Advanced Photonics*, 2020, 2(1): 015001
 99. Chin S L. *Femtosecond Laser Filamentation*. Vol. 55. New York: Springer US, 2010
 100. Docchio F. Lifetimes of plasmas induced in liquids and ocular media by single Nd:YAG laser pulses of different duration. *EPL (Europhysics Letters)*, 1988, 6(5): 407–412
 101. Feng Q, Wright E M, Moloney J V, Newell A C. Laser-induced breakdown versus self-focusing for focused picosecond pulses in water. *Optics Letters*, 1995, 20(19): 1958–1960
 102. Dai J, Zhang X C. Terahertz wave generation from gas plasma using a phase compensator with attosecond phase-control accuracy. *Applied Physics Letters*, 2009, 94(2): 021117
 103. Dorney T D, Baraniuk R G, Mittleman D M. Material parameter estimation with terahertz time-domain spectroscopy. *Journal of the Optical Society of America A, Optics, Image Science, and Vision*, 2001, 18(7): 1562–1571
 104. Babushkin I, Kuehn W, Köhler C, Skupin S, Bergé L, Reimann K, Woerner M, Herrmann J, Elsaesser T. Ultrafast spatiotemporal dynamics of terahertz generation by ionizing two-color femtosecond pulses in gases. *Physical Review Letters*, 2010, 105(5): 053903
 105. Bergé L, Skupin S, Köhler C, Babushkin I, Herrmann J. 3D numerical simulations of THz generation by two-color laser filaments. *Physical Review Letters*, 2013, 110(7): 073901
 106. Sprangle P, Peñano J R, Hafizi B, Kapetanacos C A. Ultrashort laser pulses and electromagnetic pulse generation in air and on dielectric surfaces. *Physical Review E: Statistical, Nonlinear, and Soft Matter Physics*, 2004, 69(6): 066415
 107. Ponomareva E A, Stumpf S A, Tcypkin A N, Kozlov S A. Impact of laser-ionized liquid nonlinear characteristics on the efficiency of terahertz wave generation. *Optics Letters*, 2019, 44(22): 5485–5488
 108. Tcypkin A N, Ponomareva E A, Putilin S E, Smirnov S V, Shtumpf S A, Melnik M V, E Y, Kozlov S A, Zhang X C. Flat liquid jet as a highly efficient source of terahertz radiation. *Optics Express*, 2019, 27(11): 15485–15494
 109. E Y, Jin Q, Zhang X C. Enhancement of terahertz emission by a preformed plasma in liquid water. *Applied Physics Letters*, 2019, 115(10): 101101
 110. Ponomareva E A, Tcypkin A N, Smirnov S V, Putilin S E, Yiwen E, Kozlov S A, Zhang X C. Double-pump technique-one step closer towards efficient liquid-based THz sources. *Optics Express*, 2019, 27(22): 32855–32862
 111. Huang H H, Nagashima T, Hsu W H, Juodkazis S, Hatanaka K. Dual THz wave and X-ray generation from a water film under femtosecond laser excitation. *Nanomaterials (Basel, Switzerland)*, 2018, 8(7): 523
 112. Huang H H, Nagashima T, Yonezawa T, Matsuo Y, Ng S H, Juodkazis S, Hatanaka K. Giant enhancement of THz wave emission under double-pulse excitation of thin water flow. *Applied Sciences (Basel, Switzerland)*, 2020, 10(6): 2031



Optics Graduate Project Award (2018).

E-mail: jqhust@gmail.com

Qi Jin graduated from Huazhong University of Science and Technology, China in 2012 with a B.E. degree. He received a M.S. degree (2017) and earned a Ph.D. degree (2020) in Optics from University of Rochester, USA. He was awarded James Fienup Academic Achievement Award (2016), IRMMW-THz Outstanding Student Paper (2017), and Rochester Precision



terahertz wave generation from ionized liquids, especially from liquid water.

E-mail: ye2@ur.rochester.edu

Yiwen E is a research associate of The Institute of Optics, University of Rochester, USA. She received her Ph.D. degree in Optics from University of the Chinese Academy of Sciences, China in 2017. Her main research interests are terahertz wave generation and detection, terahertz wave-matter interaction, and ultrafast optics. Currently, she focuses on the project of



Xi-Cheng Zhang, Parker Givens Chair of Optics, was Director of The Institute of Optics, University of Rochester (UR), USA, a foremost institution in optics and optical physics research and education (Jan. 2012–Jun. 2017). Prior to joining UR, he pioneered world-leading research in the field of ultrafast laser-based terahertz technology and optical physics at Rensselaer Polytechnic Institute (RPI), USA (‘92–‘12). At RPI, he is the Eric Jonsson Professor of Science; Acting Head at Department of Physics, Applied Physics & Astronomy; Professor of Electrical, Computer & System; and Founding Director of Center for THz Research. He is co-founder of Zomega Terahertz Corp. With a B.S. degree (‘82) from Peking University, China, he earned the M.S. (‘83) and Ph.D. degrees (‘86) in Physics from Brown University, USA.

Dr. Zhang served as Editor-in-Chief of *Optics Letters*, OSA (‘14–‘19). He currently serves as Executive Editor-in-Chief of *Light, Science and Applications*. He is a Fellow of AAAS, APS, IEEE, OSA, and SPIE. Previous positions included visiting scientist at MIT

(‘85), Physical Tech. Division of Amoco Research Center (‘87), EE Dept. at Columbia University (‘87–‘91); Distinguished Visiting Scientist at Jet Propulsion Laboratory, Caltech (2006), USA. He holds 29 US patents, and is a prolific author and speaker.

His honors and awards include: Humboldt Prize (‘18); Australian Academy of Science Selby Fellow (‘17); IRMMW-THz Kenneth Button Prize (‘14); OSA William F. Meggers Award (‘12); IEEE Photonics Society William Streifer Scientific Achievement Award (‘11); Rensselaer William H. Wiley 1866 Award (‘09); Japan Society for the Promotion of Science Fellowship & NRC-CIAR Distinguished Visiting Scientist, Canada (‘04); First Heinrich Rudolf Hertz Lecturer, RWTH, Aachen, Germany (‘03). He also served two years as a Distinguished Lecturer of IEEE/LEOS. He received Rensselaer Early Career Award (‘96), Research Corporation Cottrell Scholar Award (‘95), NSF Early Career Award (‘95), K.C. Wong Prize, K.C. Wong Foundation, Hong Kong (‘95), NSF Research Initiation Award (‘92). In ‘93–‘94, he was an AFOSR-SRPF Fellow at Hanscom Air Force Base.

E-mail: xi-cheng.zhang@rochester.edu